OCEANOGRAPHY

Thermal stress reduces pocilloporid coral resilience to ocean acidification by impairing control over calcifying fluid chemistry

Maxence Guillermic[1,2,3]*, Louise P. Cameron[4,5,6], Ilian De Corte[1,2], Sambuddha Misra[7,8], Jelle Bijma[9], Dirk de Beer[10], Claire E. Reymond[6,11], Hildegard Westphal[6,12], Justin B. Ries[4,6], Robert A. Eagle[1,2,3]*

The combination of thermal stress and ocean acidification (OA) can more negatively affect coral calcification than an individual stressors, but the mechanism behind this interaction is unknown. We used two independent methods (microelectrode and boron geochemistry) to measure calcifying fluid pH (pH_{cf}) and carbonate chemistry of the corals *Pocillopora damicornis* and *Stylophora pistillata* grown under various temperature and pCO_2 conditions. Although these approaches demonstrate that they record pH_{cf} over different time scales, they reveal that both species can cope with OA under optimal temperatures (28°C) by elevating pH_{cf} and aragonite saturation state (Ω_{cf}) in support of calcification. At 31°C, neither species elevated these parameters as they did at 28°C and, likewise, could not maintain substantially positive calcification rates under any pH treatment. These results reveal a previously uncharacterized influence of temperature on coral pH_{cf} regulation—the apparent mechanism behind the negative interaction between thermal stress and OA on coral calcification.

INTRODUCTION

Coral reefs are some of the most diverse and productive ecosystems on Earth. Increasing anthropogenic atmospheric CO_2 causes warming and acidification of the oceans, thereby threatening these precious ecosystems (*1*, *2*). Thermal stress causes coral bleaching, as evidenced by the increasing frequency and magnitude of mass bleaching events over the last several decades (*1*) and reduced calcification rates of corals. Ocean acidification (OA) can also impair coral calcification. Although it is well established that the combination of thermal stress and OA can more negatively affect coral calcification than either stressor alone (*3*–*5*), the mechanism behind this interaction—essential for predicting the impacts of future global change on corals—is not fully understood.

The ability of different coral species to calcify under a range of environmental conditions is partially attributed to the apparently strong control that they exert on their internal calcifying fluid (also known as the "calcifying medium") (*6*). In this study, we exposed corals to a range of pCO_2 and thermal treatments and estimated their calcifying fluid pH (pH_{cf}) from the boron isotope ($\delta^{11}B_c$) composition of their skeletal aragonite and compared it to direct pH microelectrode measurements of their calcifying fluids (*7*). We also estimated the carbonate ion concentration of the calcifying fluid ($[CO_3^{2-}]_{cf}$) from skeletal B/Ca measurements (*8*). We then used these two key measurements (pH_{cf} and $[CO_3^{2-}]_{cf}$) to calculate other carbonate system parameters of the coral calcifying fluid (DIC_{cf} and Ω_A) (*8*–*10*). Our results provide insight into the impacts of future global oceanic change (*11*) on the calcifying fluid dynamics of tropical pocilloporid corals and relate these impacts to corals' ability to produce their skeletons under future high-CO_2 and high-temperature conditions.

Background on scleractinian coral biomineralization

In a stable climate, the persistence of coral reefs relies on the capacity of corals to produce new skeleton fast enough to offset processes of skeletal degradation (e.g., dissolution and bioerosion). Many species of tropical corals maintain a symbiosis with photosynthetic algae (i.e., zooxanthellae), which yields additional energy for calcification, thereby allowing them to maintain net positive rates of skeletal accretion and, in some cases, build large reef structures. This symbiosis enables the coral host to access up to 90% of the fixed carbon they require while providing the zooxanthellae with protection and access to nutrients (nitrogen and phosphorus) and dissolved inorganic carbon (DIC).

The precipitation of aragonite is thought to occur in the subcalicoblastic space (between the base of the calicoblastic tissue and the skeleton), from a partially isolated extracellular calcifying fluid (*6*, *12*), with components of the calcifying fluid sourced from seawater (*11*) and precipitation of aragonite influenced by organic matrices (*13*).

Corals elevate the pH of their calcifying fluid under both normal and acidified conditions [e.g., (*14*)], potentially via enzymes that exchange Ca^{2+} and H^+ between seawater and the coral calcifying fluid (e.g., Ca-ATPase) (*15*). CO_2 dissolved in the coral calcifying fluid, which is derived from seawater, coral respiration (*16*), direct transport

[1]Department of Atmospheric and Oceanic Sciences, Institute of the Environment and Sustainability, University of California, Los Angeles, 520 Portola Plaza, Los Angeles, CA 90095, USA. [2]Department of Earth, Planetary, and Space Sciences, University of California, Los Angeles, 595 Charles Young Drive E, Los Angeles, CA 90095, USA. [3]Institut Universitaire Européen de la Mer, LGO, Rue Dumont d'Urville, Université de Brest Occidentale, 29280, Plouzané, France. [4]Department of Marine and Environmental Sciences, Marine Science Center, Northeastern University, 430 Nahant Rd, Nahant, MA 01908, USA. [5]McLean Laboratory, Woods Hole Oceanographic Institution,360 Woods Hole Rd, Falmouth, MA 02543, USA. [6]The Leibniz Centre for Tropical Marine Research (ZMT), Fahrenheitstraße 6, 28359 Bremen, Germany. [7]Centre for Earth Sciences, Indian Institute of Science, Bengaluru, Karnataka 560012, India. [8]The Godwin Laboratory for Palaeoclimate Research, Department of Earth Sciences, University of Cambridge, Cambridge, UK. [9]Marine Biogeosciences, Alfred-Wegener-Institut Helmholtz-Zentrum für Polar- und Meeresforschung, Am Handelshafen 12, 27570 Bremerhaven, Germany. [10]Max Planck Institute for Marine Microbiology, Celsiusstraße 1, 28359 Bremen, Germany. [11]State Key Laboratory of Biogeology and Environmental Geology, China University of Geosciences (CUG), 388 Lumo Rd, Hongshan, Wuhan 430074, P. R. China. [12]Department of Geosciences, Bremen University, 28359 Bremen, Germany.
*Corresponding author. Email: maxence.guillermic@gmail.com (M.G.); robeagle@g.ucla.edu (R.A.E.)

(*17*), and/or passive CO_2 diffusion (*12*, *18*, *19*), is converted into HCO_3^- via the enzyme carbonic anhydrase (CA) and increasing pH_{cf} (Eq. 1) (*18*). Increasing pH_{cf} also causes HCO_3^- to dissociate into H^+ and CO_3^{2-} (Eq. 1), thereby increasing the aragonite saturation state (Ω_{ar}, Eq. 2) and driving calcification via Eq. 3 (*6*)

$$CO_2 + H_2O \leftrightarrow HCO_3^- + H^+ \leftrightarrow CO_3^{2-} + 2H^+ \quad (1)$$

$$\Omega ar = \frac{[Ca^{2+}] \times [CO_3^{2-}]}{K^* sp} \quad (2)$$

$$Ca^{2+} + CO_3^{2-} \leftrightarrow CaCO_3 \quad (3)$$

Evidence has also emerged that coral skeletal growth is influenced by organic molecules, such as coral acid rich proteins (CARPs) proteins (*20*, *21*). It has also been reported that the precipitation of coral skeletal aragonite may be preceded by a transient phase of amorphous calcium carbonate (ACC) (*22*, *23*). Although the ACC-to-aragonite transformation could introduce complexity into the interpretation of geochemical proxies recorded in coral skeletons, one would still expect the geochemistry of the aragonite skeleton to reflect conditions at the site of calcification and, to some extent, seawater, since the transformation of ACC to aragonite may occur within the high-pH and high-Ω extracellular coral calcifying fluid where nucleating aragonite crystals are observed [e.g., (*24*)] and involve dissolution and reprecipitation of the ACC in that fluid (*25*). However, the role of ACC in coral calcification is an ongoing debate (*23*, *26*–*28*) and, like the potential role of organic molecules in coral calcification, does not materially affect interpretation of the present study.

Boron incorporation and isotope fractionation in coral aragonite

Previous studies support the assertion that $B(OH)_4^-$ is the primary form of boron incorporated into coral aragonite (*29*). Inorganic $CaCO_3$ precipitation experiments suggest that $B(OH)_4^-$ is substituted for CO_3^{2-} in the aragonite lattice (*30*, *31*). Prior studies also suggest that $[CO_3^{2-}]_{cf}$ can be estimated from coral skeletal B/Ca [see (*8*) for a review]. However, several substitution equations have been proposed to maintain charge balance when substituting $B(OH)_4^-$ for CO_3^{2-} in aragonite, resulting in divergent definitions for the B/Ca partition coefficient K_D (*8*, *10*). The K_D defined below (Eq. 4) (*10*) was used to calculate carbonate system parameters in the present study pursuant to the rationale provided in (*8*) and because our reconstructed $[CO_3^{2-}]_{cf}$ following the rationale in (*10*) was consistent with independent electrode $[CO_3^{2-}]_{cf}$ (fig. S1) (*32*)

$$K_D = \frac{B/Ca}{[B(OH)_4^-]/[CO_3^{2-}]_{cf}} \quad (4)$$

Nevertheless, carbonate system parameters calculated from a range of published K_D equations are also presented (table S1) to acknowledge the ongoing research in this area (*8*, *10*, *33*, *34*). The main outcomes of this study are preserved whatever K_D formulation is used.

Controlled laboratory experiments on corals have revealed that $\delta^{11}B$ of the coral skeleton, relative to borate $\delta^{11}B$ of the organism's surrounding seawater, is higher than skeletal $\delta^{11}B$ of most other species of marine calcifiers (*35*, *36*). Thus, the $\delta^{11}B$ composition of coral aragonite likely reflects pH of the calcifying fluid, which, in corals, is known from independent measurements [microelectrode and pH-sensitive dye; e.g., (*14*, *37*)] to be substantially elevated relative to seawater pH (pH_{sw}). Numerous studies have used this apparent relationship to estimate coral's pH_{cf} from their skeletal $\delta^{11}B$ to explore the ability of corals to regulate their pH_{cf} in response to environmental stress, as summarized below.

Modification of coral calcifying fluid chemistry under future global change scenarios

Response of calcifying fluid to OA

Various experimental studies have used coral skeletal $\delta^{11}B$ to examine the ability of scleractinian corals to modify pH of their calcifying fluid under normal and acidified conditions [see (*38*) for a review]. These studies reveal that corals increase their internal pH_{cf} relative to pH_{sw} by 0.2 to 1.1 units, with the offset generally increasing with the degree of acidification. These observations are consistent with other observations of elevated pH_{cf} based on pH microsensors and pH-sensitive dyes (*37*, *39*–*42*). The $\delta^{11}B$ approach reveals that the sensitivity of pH_{cf} to pH_{sw} ($\Delta pH_{cf}/\Delta pH_{sw}$) in culture experiments on zooxanthellae-bearing corals ranges across species from 0.23 to 0.51 (*38*). However, corals in their natural environment appear to exhibit greater sensitivity in $\delta^{11}B$-based estimates of pH_{cf} to pH_{sw} than corals cultured in laboratory experiments (*10*).

A study on *Stylophora pistillata* (*42*) used controlled laboratory experiments at a single temperature of 25°C to show that changes in DIC_{sw} affected pH_{cf} and DIC_{cf}. Such findings have also been observed in natural environments, where changes in pH_{cf} and DIC_{cf} modulate Ω_{cf} in support of coral calcification (*9*, *10*). In one of the few coral-$\delta^{11}B$ studies conducted on a natural reef system, a *Porites* species was observed to elevate pH_{cf} by 0.4 relative to pH_{sw} (*10*), with seasonal variations of ±0.25. It was also observed that pH_{cf} and DIC_{cf} were strongly inversely correlated (*10*, *43*), with maximum pH_{cf}/minimum DIC_{cf} occurring in winter and minimum pH_{cf}/maximum DIC_{cf} occurring in summer—effectively dampening thermally induced seasonal variability in Ω_{sw}.

Response of calcifying fluid to thermal stress

Increasing atmospheric pCO_2 causes ocean warming (*11*), which negatively affects zooxanthellate corals by breaking down the coral-algal symbiosis ["bleaching"; e.g., (*1*, *44*), among many others]. Depending on the magnitude and duration of thermal stress, recovery from reduced rates of growth and reproduction accompanying bleaching events can take days to years (*45*), which may ultimately lead to the collapse of the coral reef ecosystem.

Despite the established impacts of ocean warming on coral bleaching, the impact of thermal stress on the calcifying fluid of corals is not well understood. There is some evidence from field experiments that seasonal changes in water temperature (up to 6°C) are associated with changes in calcifying fluid chemistry (DIC_{cf}, pH_{cf}, and Ω_{cf}) (*10*), as summarized above. Furthermore, the calcifying fluid of a *Porites* coral located in the central Great Barrier Reef (GBR) exhibited decoupling of pH_{cf} from DIC_{cf} (i.e., both pH_{cf} and DIC_{cf} decreased), along with decreased growth during the severe bleaching event of 1998 that caused localized bleaching of ca. 60% of zooxanthellate corals (*46*). D'Olivo *et al.* (*47*) analyzed a core obtained from a *Porites* colony from the GBR and attempted to decouple the long-term impacts of OA and warming on coral pH_{cf}. They concluded that both

processes caused pH_{cf} to decline but found that the decline due to temperature was much less than the decline due to OA—which they attributed to the species' annual exposure to large seasonal temperature changes rendering it more tolerant of thermal stress. However, it is challenging to unequivocally attribute changes in calcifying fluid chemistry to discrete oceanographic parameters owing to covariation of these parameters in the field.

RESULTS AND DISCUSSION

The skeletons of two species of pocilloporid tropical corals (*Pocillopora damicornis* and *S. pistillata*) grown under a suite of controlled temperature and pCO_2 treatments [28°C/462 parts per million (ppm), 28°C/931 ppm, 28°C/2884 ppm, 31°C/483 ppm, 31°C/908 ppm, and 31°C/3303 ppm; Table 1] were analyzed for $\delta^{11}B$ and B/Ca to gain insight into the impacts of temperature and pH_{sw} stress on coral calcifying fluid chemistry. These observations are compared to pH_{cf} microelectrode data reported elsewhere (*7*) obtained from the same individuals under the same experimental treatments. Although thermal stress is known to be the main cause of coral bleaching, no prior study has examined the combined impacts of temperature and pH_{sw} on the carbonate chemistry of coral calcifying fluid under controlled laboratory conditions.

Coral calcification response to pH_{sw} and thermal stress

Net calcification, defined here as the difference between gross calcification and gross dissolution of the coral skeleton, was estimated from the buoyant weight technique (see Materials and Methods). The corals investigated in this study generally exhibited an increase in net calcification in response to OA under both temperature conditions—with the exception of *S. pistillata* exhibiting stable (but very low) calcification rates across pH treatments under the high-temperature treatment. Both species also exhibited a decrease in net calcification with increasing temperature under each of the three pCO_2 treatments (Fig. 1, A and B) (*4*).

Corals typically exhibit parabolic, rather than linear, growth responses to temperature (*48*), referred to as thermal performance curves. Coral thermal performance curves vary across species (*7*, *49*–*51*) and may be influenced by various factors, including the environment (*52*), factors influencing photosynthesis activity (e.g., symbiont density), and symbiont clade (*53*). Prolonged thermal stress also causes bleaching, leading to reduction or cessation of calcification. Thermal performance curves previously established for the species investigated here, but collected from different areas, suggest optimal temperatures of 28° to 30°C (*48*) for *S. pistillata* and 27°C (*54*) for *P. damicornis*.

Although thermal stress reduced net calcification rates of both species (Fig. 1, A and B) (*4*), *S. pistillata* exhibited greater resilience than *P. damicornis* to thermal stress to the extent that *S. pistillata* maintained mildly positive net rates of calcification rates under the high-temperature treatments, while *P. damicornis* exhibited net dissolution.

Controlled laboratory experiments have shown that tropical scleractinian corals can exhibit a range of calcification response to OA, including linear negative, threshold negative, and parabolic (*49*, *55*, *56*). Previous OA experiments (each conducted at only a single temperature) on the two species investigated here identified different trends than observed in the present study—*S. pistillata* exhibited declining calcification with increasing pCO_2 (*57*), while *P. damicornis* exhibited no significant calcification response to pCO_2 (*9*). In the present study, both *S. pistillata* and *P. damicornis* exhibited increasing calcification rates with increasing pCO_2, except for *S. pistillata* that exhibited stable calcification rates at 31°C.

It is difficult to deconvolve the parameters responsible for the different outcomes of these experiments, as coral genetics (i.e., population), laboratory environment, feeding, light, and temperature inevitably differed among studies (*58*). For example, specimens used in these three studies were collected from different places, including from Eilat, Israel [*S. pistillata*; (*57*)], Salmon Bay, Western Australia [*P. damicornis*; (*9*)], and Fiji Islands (present study)—raising the possibility that local, population-level adaptations to temperature and pH_{sw} contributed to these differing results. Temperatures were substantially different among the experiments, suggesting that they were at least partly responsible for the different responses to OA observed in the various studies. Specifically, Comeau *et al.* (*9*) used a temperature of 21°C for *P. damicornis*, while Krief *et al.* (*57*) used a temperature of 25°C for *S. pistillata*, both below the thermal optimum for these species, compared with the substantially higher temperatures of 28°C (i.e., thermal optimum) and 31°C (above thermal optimum). Thermal optimum might also vary depending of the environment and local conditions (*52*). However, collectively, these results raise the possibility that these corals' response to OA is most resilient under their thermal optimum (28°C) and becomes more negative as temperature departs, positively (31°C) or negatively (21°C, 25°C), from this thermal optimum—although this hypothesis requires further investigation.

Response of calcifying fluid chemistry to thermal stress

pH_{cf}

The $\delta^{11}B$ measurements for *S. pistillata* were performed independently in two laboratories for the purpose of interlaboratory validation and to ensure quality control of the data (fig. S2; see also Materials and Methods and Supplemental Information). For all treatments, the mean $\delta^{11}B$ values obtained by the two laboratories for the same coral specimens were not significantly different from each other ($P > 0.05$). Likewise, slopes of the linear regressions (LRs) relating treatment condition to coral skeletal $\delta^{11}B$ obtained by the two laboratories were also not statistically different ($P > 0.05$). Last, the slope of the LR relating skeletal $\delta^{11}B$ obtained by the two laboratories for all coral specimens is not significantly different from 1 ($P = 0.39$), and the intercept is not significantly different from 0 ($P = 0.83$). It should be noted that measurements were performed on different subsamples of the same coral specimens, meaning that the small, nonsignificant differences in $\delta^{11}B$ obtained by the two laboratories may be partly attributable to small variations in $\delta^{11}B$ within the coral skeleton. These results cross-validate the $\delta^{11}B$ analytical procedures of both laboratories and show that the reported $\delta^{11}B$ values are reproducible for both laboratories at the 95% confidence level.

Both species exhibit a significant decrease in $\delta^{11}B$ with increasing temperature ($P < 0.05$) (Fig. 1, C and D), indicating that the ability of both species to elevate pH_{cf} in support of calcification is impaired under thermal stress (Fig. 1, E and F). Furthermore, both species also exhibited greater interspecimen variability in $\delta^{11}B$ within the same pCO_2 treatment at 31°C than at 28°C (Fig. 1, fig. S3, and Tables 2 and 3), with the greatest $\delta^{11}B$ variability exhibited by *P. damicornis* at 31°C. Higher interspecimen variability in $\delta^{11}B$ at 31°C provides further support for the assertion that both species exert less control over pH_{cf} under conditions of thermal stress.

Table 1. Measured and calculated seawater parameters (±SE) from the culturing experiments (*S*, salinity; *T*, temperature; pH (NBS scale); DIC, dissolved inorganic carbon; Alkalinity, total alkalinity; pH on total scale; $[CO_3^{2-}]$, carbonate ion; $[HCO_3^-]$, bicarbonate ion; $[CO_2]$, partial pressure of CO_2; Ω_A, saturation state of seawater with respect to aragonite).

Experiment	Seawater measured parameters					
	$\delta^{11}B_{sw}$* (‰)	*S* (psu)	*T* (°C)	pH (NBS scale)	DIC (μmol/kg-seawater)	Alkalinity (μmol/kg-seawater)
Exp1 (400 ppm, 28°C)	41.02 ± 0.49	34.9 ± 0.1	28.29 ± 0.01	8.27 ± 0.01	2480 ± 40	2915 ± 49
Exp2 (400 ppm, 31°C)	40.17 ± 0.33	35.6 ± 0.1	31.72 ± 0.06	8.24 ± 0.01	2350 ± 44	2774 ± 54
Exp3 (1000 ppm, 28°C)	41.36 ± 0.13	35.4 ± 0.1	27.88 ± 0.02	8.04 ± 0.01	2645 ± 44	2939 ± 46
Exp4 (1000 ppm, 31°C)	41.93 ± 0.20	36.0 ± 0.1	30.83 ± 0.02	8.12 ± 0.01	2755 ± 37	3083 ± 40
Exp5 (2800 ppm, 28°C)	40.97 ± 0.15	35.8 ± 0.1	28.17 ± 0.02	7.62 ± 0.01	2861 ± 82	2907 ± 81
Exp6 (2800 ppm, 31°C)	41.35 ± 0.12	35.7 ± 0.1	30.93 ± 0.02	7.69 ± 0.01	3223 ± 57	3290 ± 56

Experiment	Seawater calculated parameters					
	pCO_2 (ppmv)	pH** (total scale)	$[CO_3^{2-}]$ (μmol/kg-seawater)	$[HCO_3^-]$ (μmol/kg-seawater)	$[CO_2]$ (μmol/kg-seawater)	Ω_A
Exp1 (400 ppm, 28°C)	466 ± 8	8.14 ± 0.01	334 ± 9	2133 ± 33	12.3 ± 0.2	5.38 ± 0.14
Exp2 (400 ppm, 31°C)	499 ± 9	8.09 ± 0.01	320 ± 11	2017 ± 36	12.3 ± 0.3	5.20 ± 0.18
Exp3 (1000 ppm, 28°C)	925 ± 15	7.90 ± 0.01	217 ± 6	2424 ± 35	24.6 ± 0.4	3.48 ± 0.10
Exp4 (1000 ppm, 31°C)	885 ± 12	7.97 ± 0.01	265 ± 4	2468 ± 35	22.0 ± 0.4	4.28 ± 0.07
Exp5 (2800 ppm, 28°C)	2807 ± 120	7.49 ± 0.01	90 ± 3	2697 ± 77	74.3 ± 3.2	1.44 ± 0.04
Exp6 (2800 ppm, 31°C)	3194 ± 136	7.55 ± 0.01	113 ± 4	3030 ± 54	79.5 ± 3.4	1.83 ± 0.06

*$\delta^{11}B_{sw}$-based average of $\delta^{11}B_{sw1}$ and $\delta^{11}B_{sw2}$ (see table S5) for each condition during experiment. **pH on total scale recalculated on the basis of pH measured on NBS scale during experiment.

The pH_{cf} was also measured with pH microelectrodes both in the light (pH_{cf_light}) and in the dark (pH_{cf_dark}) (Fig. 1, E and F). Both pH_{cf_light} and pH_{cf_dark} yielded an inverse correlation between temperature and pH_{cf}. However, microelectrode measurements of pH_{cf_light} and pH_{cf_dark} were respectively significantly ($P < 0.05$) greater and less than pH_{cf} measured via $\delta^{11}B$. In addition, despite the offset in the $\delta^{11}B$-based and microelectrode-based measurements of pH_{cf}, temperature-driven decreases in pH_{cf} (e.g., $\Delta pH_{cf}/\Delta T$) detected by the two approaches did not significantly differ from each other under any of the pCO_2 treatments [*S. pistillata* at 400 ppm ($P = 0.86$), at 1000 ppm ($P = 0.35$), and at 2800 ppm ($P = 0.54$)] (Figs. 1F and 2).

The impact of OA on pH_{cf} was more complex than the impact of temperature discussed above. Both species under 28°C and *S. pistillata* under 31°C exhibited homeostatic pH_{cf} responses to seawater acidification—i.e., pH_{cf} remained relatively constant with declining pH_{sw}. In contrast, *P. damicornis* under 31°C exhibited pH_{cf} that tracks pH_{sw}, meaning that the coral is not able to maintain pH_{cf} homeostasis. Under pH_{cf}-homeostatic conditions (both species under 28°C and *S. pistillata* under 31°C), the corals elevate pH_{cf} by up to 0.7 units relative to pH_{sw}, with the greatest increase in pH_{cf} (relative to pH_{sw}) exhibited under the lowest pH_{sw} treatment. Thus, under more acidic conditions, the corals elevate pH_{cf} more, relative to pH_{sw}, than under less acidic conditions—at potentially increased energetic cost to the organism [e.g., (*14*)]. *P. damicornis* seems to lose this compensatory ability under thermal stress (31°C).

The sensitivity of pH_{cf} to temperature is also seen in the pH microelectrode data. Again, despite the difference in absolute measured pH_{cf} between the $\delta^{11}B$ and microelectrode approaches, pH_{sw}-driven changes in pH_{cf} (e.g., $\Delta pH_{cf}/\Delta pH_{sw}$) detected by the two approaches did not significantly differ from each other for either species under any of the temperature treatments (*P. damicornis* at 28°C, $P = 0.14$; *S. pistillata* at 28°C, $P = 0.06$; *S. pistillata* at 31°C, $P = 0.72$; Fig. 1, E and F). Absolute differences in measured pH_{cf} between the two approaches are discussed further in the "Fidelity of coral skeletal $\delta^{11}B$ in recording coral pH_{cf}" section.

The observations that *S. pistillata* is able to maintain pH_{cf} homeostasis under acidified conditions under both temperatures and that *P. damicornis* can only maintain pH_{cf} homeostasis under the control (optimal) temperature suggest that *P. damicornis* is more susceptible to this apparent negative interaction between thermal stress and OA. Despite the inability of *P. damicornis* at 31°C to elevate pH_{cf} above pH_{sw} in support of calcification, gross calcification (but not net calcification) was still occurring, as indicated by the discrete calcein dye layer that was recorded in the coral skeleton to identify new skeletal material for boron isotopic and elemental analysis. This supports previous assertions that the saturation state of the coral calcifying fluid can be increased in support of calcification by increasing DIC_{cf} while maintaining pH_{cf} that is elevated relative to the equilibrium pH_{cf} expected from the elevated DIC_{cf} (even if pH_{cf} tracks pH_{sw}) (*9*) and also that organic templates and organic molecules within the calcifying fluid may support the coral calcification process [e.g., (*59*)].

$[CO_3^{2-}]_{cf}$ and DIC_{cf}

Our results also show that both coral species elevate $[CO_3^{2-}]_{cf}$ and DIC_{cf} relative to the corals' surrounding seawater under all treatment conditions (Fig. 2 and Tables 2 and 3). Furthermore, both species maintain a relatively constant $[CO_3^{2-}]_{cf}$ across pCO_2 treatments

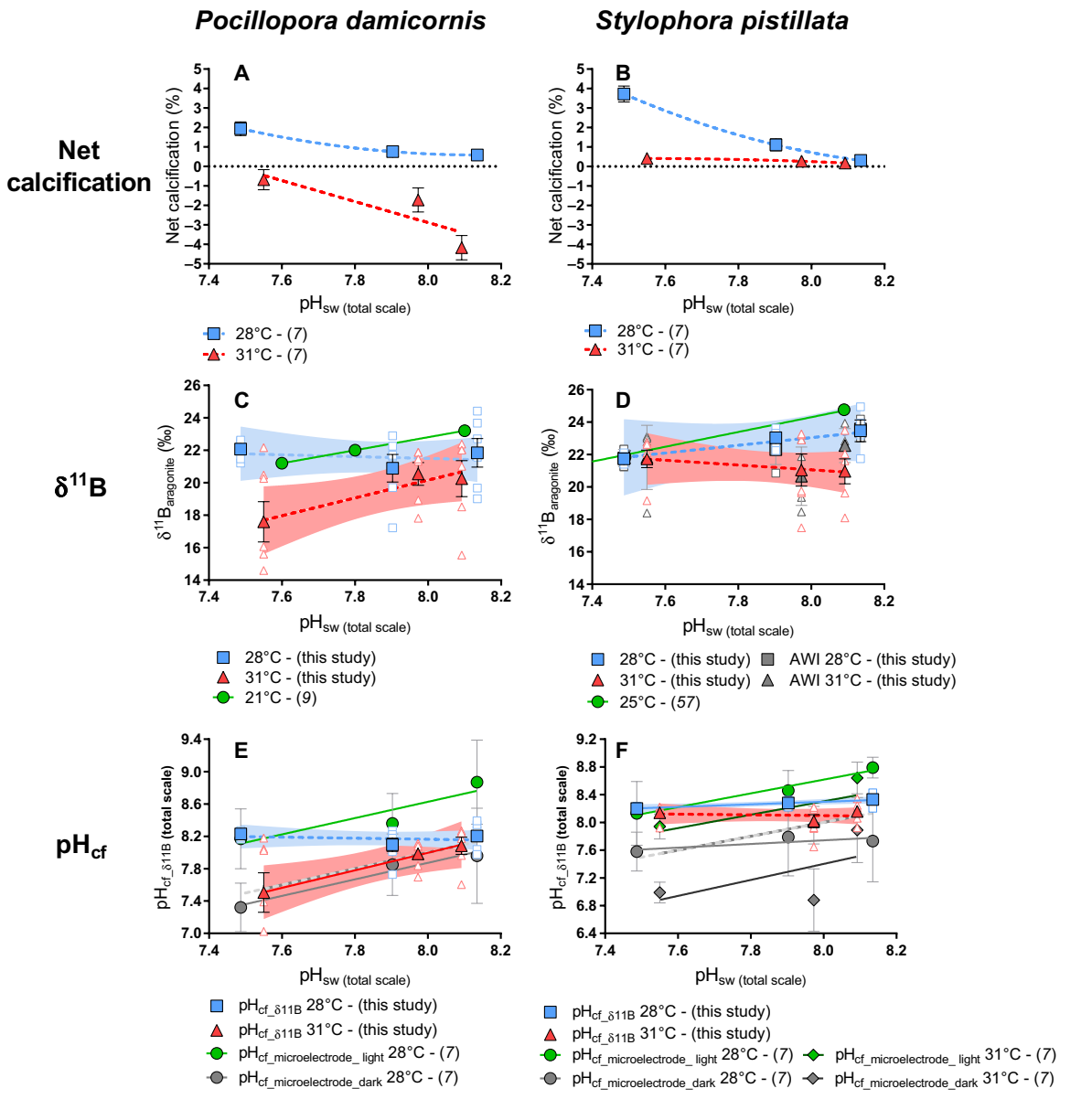

Fig. 1. Calcifying fluid pH_{cf}-based boron isotopes. Panels show measured parameters as a function of treatment pH_{sw}. Blue squares correspond to 28°C, red triangles correspond to 31°C, solid symbols represent treatment averages, and open symbols represent data for individual coral specimens. (**A**) and (**B**) show net calcification rate as percent change in skeletal mass throughout the experiment (*7*). (**C**) and (**D**) show $\delta^{11}B$ measured for *P. damicornis* and *S. pistillata*, respectively, and independent measurements of $\delta^{11}B$ of *S. pistillata* by Alfred Wegener Institute for Polar and Marine Research (AWI), with individuals shown in open dark gray and treatment averages shown in solid gray. Dotted horizontal lines represent zero calcification. (**E**) and (**F**) show calculated pH_{cf} (see the main text) for *P. damicornis* and *S. pistillata*, respectively. Best-fit model (linear or nonlinear regressions) was determined using GraphPad based on lowest akaike information criteria (AIC); solid lines indicate significant regressions. Dashed gray lines represent 1:1 ratio of pH_{cf}:pH_{sw} for comparison to observed trends (28°C, dark; 31°C, light). Error bars are given in SEM and envelopes for the regressions represent 95% confidence interval.

($P = 0.53$ for *S. pistillata* at 28°C, $P = 0.27$ for *S. pistillata* at 31°C, $P = 0.52$ for *P. damicornis* at 28°C, and $P = 0.30$ for *P. damicornis* at 31°C), resulting in a large increase in $[CO_3^{2-}]_{cf}$ relative to $[CO_3^{2-}]_{sw}$ in the lowest pH_{sw} treatment (Fig. 2, C and D). Although *P. damicornis* at 31°C exhibits an apparent decline in $[CO_3^{2-}]_{cf}$ with decreasing pH_{sw}, this trend was not statistically significant ($P = 0.2$). In contrast, DIC_{cf} trends differed between the two species, with *S. pistillata* exhibiting increasing DIC_{cf} with decreasing pH_{sw} at 28°C [LR: $R^2 = 0.84$, $P = 0.09$; analysis of variance (ANOVA): $P < 0.0001$] and 31°C (LR: $R^2 = 0.31$, $P = 0.01$; ANOVA: $P = 0.05$), and with *P. damicornis* exhibiting constant DIC_{cf} with decreasing pH_{sw} at 28°C (LR: $R^2 = 0.22$, $P = 0.53$; ANOVA: $P = 0.08$) and 31°C (LR: $R^2 = 0.15$, $P = 0.12$; ANOVA: $P = 0.69$). However, both species exhibited DIC_{cf} that was significantly ($P < 0.05$) elevated relative to DIC_{sw} in each treatment, except for *P. damicornis* at 31°C that exhibited DIC_{cf} that was statistically indistinguishable from DIC_{sw} at 1000 and 2800 ppm ($P = 0.16$). Furthermore, both species exhibited lower $[CO_3^{2-}]_{cf}$ and DIC_{cf} under conditions of thermal stress but only under the highest pCO_2 treatment (Figs. 2 and 3; $[CO_3^{2-}]_{cf}$: $P = 0.02$ for both species; DIC_{cf}: $P = 0.05$ for *P. damicornis*; $P = 0.01$ for *S. pistillata*).

Table 2. Measured values of $\delta^{11}B$ and elemental ratios (B/Ca) within the skeletons of *P. damicornis* and corresponding reconstructed parameters of the calcifying fluid (pH_{cf}, $[CO_3^{2-}]_{cf}$, and DIC_{cf}).

Culture conditions				Analytical results				Calculated parameters		
pCO_{2sw}	T	pH_{sw}	Tank	$\delta^{11}Bc_1$ (±2 SD)	$\delta^{11}Bc_2$ (±2 SD)	$\delta^{11}B_{average}$ (±2 SD)	B/Ca (±2 SD)	pH_{cf}	$[CO_3^{2-}]_{cf}$ (±1 SE)	DIC_{cf} (±1 SE)
(ppm)	(°C)	(total scale)		(‰)	(‰)	(‰)	(μmol/mol)	(total scale)	(μmol/kg)	(μmol/kg)
Pocillopora damicornis										
466	28	8.14	1	19.70 ± 0.10	19.65 ± 0.10	19.68 ± 0.07	472 ± 11	8.04	522 ± 66	4458 ± 199
466	28	8.14	2	21.52 ± 0.10	21.63 ± 0.10	21.58 ± 0.07	545 ± 11	8.19	621 ± 57	3891 ± 162
466	28	8.14	3	22.76 ± 0.10	22.65 ± 0.10	22.71 ± 0.07	449 ± 11	8.28	877 ± 70	4694 ± 206
466	28	8.14	4	23.67 ± 0.11	23.68 ± 0.11	23.68 ± 0.08	492 ± 11	8.34	894 ± 65	4240 ± 175
466	28	8.14	1	24.42 ± 0.39		24.42 ± 0.39	489 ± 11	8.39	975 ± 76	4231 ± 178
466	28	8.14	2	19.01 ± 0.39		19.01 ± 0.39	460 ± 11	7.97	463 ± 81	4513 ± 222
499	31	8.09	4	22.02 ± 0.21	22.09 ± 0.21	22.06 ± 0.29	537 ± 11	8.25	759 ± 61	3840 ± 157
499	31	8.09	4	22.38 ± 0.09		22.38 ± 0.09	537 ± 11	8.27	789 ± 55	3834 ± 162
499	31	8.09	1	21.02 ± 0.09		21.02 ± 0.09	501 ± 11	8.17	707 ± 57	4130 ± 176
499	31	8.09		22.01 ± 0.11	22.02 ± 0.11	22.01 ± 0.08	500 ± 11	8.24	809 ± 57	4126 ± 174
499	31	8.09	3	18.53 ± 0.11	18.50 ± 0.11	18.51 ± 0.08	504 ± 11	7.96	455 ± 58	4000 ± 188
499	31	8.09	4	15.56 ± 0.11	15.53 ± 0.11	15.55 ± 0.08	470 ± 11	7.60	184 ± 60	3459 ± 461
925	28	7.90	2	17.22 ± 0.11	17.23 ± 0.11	17.23 ± 0.08	435 ± 11	7.73	263 ± 58	4329 ± 339
925	28	7.90	1	19.78 ± 0.11	19.63 ± 0.11	19.71 ± 0.08	558 ± 11	8.01	422 ± 45	3807 ± 162
925	28	7.90	3	22.98 ± 0.26	22.82 ± 0.26	22.90 ± 0.18	492 ± 11	8.27	800 ± 55	4361 ± 178
925	28	7.90	2	22.25 ± 0.09		22.25 ± 0.09	491 ± 11	8.22	735 ± 54	4383 ± 185
925	28	7.90	4	21.60 ± 0.09		21.60 ± 0.09	503 ± 11	8.17	652 ± 54	4280 ± 178
925	28	7.90	1	21.69 ± 0.09		21.69 ± 0.09	619 ± 11	8.18	538 ± 42	3482 ± 136
885	31	7.97	4	21.32 ± 0.09		21.32 ± 0.09	743 ± 11	8.07	387 ± 38	2812 ± 114
885	31	7.97	3	18.94 ± 0.09		18.94 ± 0.09	474 ± 11	7.84	356 ± 56	4141 ± 230
885	31	7.97	1	21.89 ± 0.21	21.85 ± 0.21	21.87 ± 0.15		8.11		
885	31	7.97	3	21.88 ± 0.09		21.88 ± 0.09	592 ± 11	8.11	533 ± 46	3550 ± 146
885	31	7.97	3	17.84 ± 0.11	17.80 ± 0.11	17.82 ± 0.08	524 ± 11	7.70	217 ± 50	3422 ± 286
885	31	7.97	1	21.47 ± 0.11	21.46 ± 0.11	21.46 ± 0.08	441 ± 11	8.08	668 ± 61	4751 ± 208
2807	28	7.49	1	22.59 ± 0.26	22.53 ± 0.26	22.56 ± 0.18	460 ± 11	8.27	865 ± 60	4673 ± 192
2807	28	7.49	4	22.60 ± 0.11	22.35 ± 0.11	22.48 ± 0.08	466 ± 11	8.26	845 ± 57	4613 ± 187
2807	28	7.49	3	21.19 ± 0.11	21.24 ± 0.11	21.21 ± 0.08	422 ± 11	8.17	782 ± 64	5118 ± 224
2807	28	7.49	2	22.69 ± 0.11	22.57 ± 0.11	22.63 ± 0.08	496 ± 11	8.27	811 ± 54	4339 ± 175
2807	28	7.49	2	21.48 ± 0.21		21.48 ± 0.21		8.19		
3194	31	7.55	4	22.17 ± 0.39		22.17 ± 0.39	485 ± 11	8.18	734 ± 69	4300 ± 178
3194	31	7.55	2	20.47 ± 0.09		20.47 ± 0.09	486 ± 11	8.04	557 ± 53	4266 ± 184
3194	31	7.55	3	15.61 ± 0.09		15.61 ± 0.09	538 ± 11	7.39	74 ± 7[x]	2276 ± 108
3194	31	7.55	4	16.06 ± 0.09		16.06 ± 0.09	518 ± 11	7.49	113 ± 46	2774 ± 94
3194	31	7.55	1	14.60 ± 0.11	14.59 ± 0.11	14.60 ± 0.08	449 ± 11	7.02	14 ± 4[x]	950 ± 175
3194	31	7.55	4	20.24 ± 0.11	20.29 ± 0.11	20.26 ± 0.08	509 ± 11	8.02	512 ± 50	4061 ± 180
3194	31	7.55	2	14.00 ± 0.11	13.94 ± 0.11	13.97 ± 0.08	523 ± 11	6.38		

pCO_{2sw}, seawater pCO_2 of the culture treatment. T, seawater temperature of the culture treatment. pH_{sw}, seawater pH of the culture treatment. Tank, tank number where the sample was cultured. $\delta^{11}Bc_1$, first measurement of the boron isotopic composition of the sample, uncertainty determined on reproducibility of the AE121 standard (2 SD). $\delta^{11}Bc_2$, duplicate analysis of the boron isotopic composition of the sample, uncertainty determined on reproducibility of the AE121 standard (2 SD). $\delta^{11}B_{average}$, average of $\delta^{11}B_{c1}$ and $\delta^{11}B_{c2}$ or $\delta^{11}B_{c1}$ if only one measurement was performed. When two measurements were carried out, uncertainty was calculated based on uncertainties of $\delta^{11}B_{c1}$ and $\delta^{11}B_{c2}$ ($\Delta a = \sqrt{(\Sigma i(\Delta ai)^2)}$). B/Ca measured for the sample. Uncertainty is calculated as 2 SD of repeated measurements of the CamWuellestorfi standard (table S4). pH_{cf} calculated from $\delta^{11}B$ using (*8*) based on Monte Carlo simulation. $[CO_3^{2-}]_{cf}$ calculated from B/Ca using (*8*). DIC_{cf} calculated from $\delta^{11}B$ and B/Ca using (*8*). Uncertainties for $[CO_3^{2-}]$cf and DIC_{cf} calculated using (*8*), Δ (1 SE) = $\sqrt{(\Sigma i(\Delta sysi + \Delta nonsysi)^2)}$, [x]uncertainty = Δnonsys (1 SE). Additional data not used in this study (Li/Ca, Mg/Ca and Sr/Ca) are presented in table S7 in the Supplementary Materials.

Table 3. Measured values of $\delta^{11}B$ and elemental ratios (B/Ca) within the skeletons of *S. pistillata* and corresponding reconstructed parameters of the calcifying fluid (pH_{cf}, $[CO_3^{2-}]_{cf}$, and DIC_{cf}).

Culture conditions				Analytical results						
pCO_{2sw}	*T*	pH_{sw}	Tank	$\delta^{11}Bc_1$ (±2 SD)	$\delta^{11}Bc_2$ (±2 SD)	$\delta^{11}B_{average}$ (±2 SD)	B/Ca (±2 SD)	pH_{cf}	$[CO_3^{2-}]_{cf}$ (±1 SE)	DIC_{cf} (±1 SE)
(ppm)	(°C)	(total scale)		(‰)	(‰)	(‰)	(μmol/mol)	(total scale)	(μmol/kg)	(μmol/kg)
Stylophora pistillata										
466	28	8.14	2	23.20 ± 0.30	23.21 ± 0.30	23.20 ± 0.21	470 ± 11	8.31	888 ± 70	4464 ± 191
466	28	8.14	2				455 ± 11		918 ± 71	4614 ± 194
466	28	8.14	2				459 ± 11		909 ± 70	4584 ± 190
466	28	8.14	4	21.85 ± 0.30	21.63 ± 0.30	21.74 ± 0.21	527 ± 11	8.21	659 ± 62	4021 ± 166
466	28	8.14	1	23.95 ± 0.26		23.95 ± 0.26	432 ± 11	8.36	1050 ± 78	4815 ± 216
466	28	8.14	2	24.94 ± 0.26		24.94 ± 0.26	480 ± 11	8.43	1048 ± 70	4291 ± 181
499	31	8.09	2	18.09 ± 0.26		18.09 ± 0.26	378 ± 11	7.92	553 ± 84	5283 ± 284
499	31	8.09	4	21.62 ± 0.09		21.62 ± 0.09	536 ± 11	8.21	718 ± 54	3850 ± 163
499	31	8.09	1	23.48 ± 0.09		23.48 ± 0.09	513 ± 11	8.34	934 ± 59	3968 ± 163
499	31	8.09	1				526 ± 11		983 ± 63	4179 ± 184
499	31	8.09	4	20.93 ± 0.26		20.93 ± 0.26	411 ± 11	8.16	851 ± 79	5046 ± 231
499	31	8.09	3	19.62 ± 0.09		19.62 ± 0.09	462 ± 11	8.06	616 ± 63	4451 ± 203
499	31	8.09	1	22.04 ± 0.09		22.04 ± 0.09	557 ± 11	8.24	728 ± 53	3692 ± 160
499	31	8.09	1				473 ± 11		859 ± 62	4351 ± 187
925	28	7.90	2	23.26 ± 0.36		23.26 ± 0.36	419 ± 11	8.29	980 ± 77	5097 ± 217
925	28	7.90	4	22.70 ± 0.26		22.70 ± 0.26	440 ± 11	8.25	870 ± 67	4885 ± 207
925	28	7.90	1	22.25 ± 0.26		22.25 ± 0.26	451 ± 11	8.22	800 ± 64	4770 ± 204
925	28	7.90	3	23.63 ± 0.26		23.63 ± 0.26	449 ± 11	8.32	958 ± 67	4747 ± 200
925	28	7.90	2	23.32 ± 0.26		23.32 ± 0.26	485 ± 11	8.30	855 ± 62	4403 ± 184
885	31	7.97	3	23.01 ± 0.21	22.79 ± 0.21	22.90 ± 0.15		8.19		
885	31	7.97	1	23.21 ± 0.39		23.21 ± 0.39	417 ± 11	8.21	920 ± 82	5038 ± 220
885	31	7.97	3	19.64 ± 0.26		19.64 ± 0.26	378 ± 11	7.91	541 ± 79	5346 ± 286
885	31	7.97	4	19.76 ± 0.26		19.76 ± 0.26	595 ± 11	7.92	353 ± 50	3408 ± 161
885	31	7.97	1	17.49 ± 0.26		17.49 ± 0.26	394 ± 11	7.65	251 ± 73	4347 ± 474
885	31	7.97	2	23.27 ± 0.39		23.27 ± 0.39	417 ± 11	8.22	929 ± 84	5036 ± 219
2807	28	7.49	3	22.11 ± 0.39		22.11 ± 0.39	384 ± 11	8.23	983 ± 86	5622 ± 251
2807	28	7.49	3	21.90 ± 0.39		21.90 ± 0.39	377 ± 11	8.22	968 ± 86	5726 ± 257
2807	28	7.49	4	21.51 ± 0.39		21.51 ± 0.39	357 ± 11	8.19	969 ± 94	6046 ± 287
2807	28	7.49	4	21.40 ± 0.39		21.40 ± 0.39	355 ± 11	8.18	958 ± 95	6095 ± 286
3194	31	7.55	4	21.74 ± 0.39		21.74 ± 0.39	410 ± 11	8.15	819 ± 81	5101 ± 231
3194	31	7.55	2	22.75 ± 0.39		22.75 ± 0.39	425 ± 11	8.22	903 ± 79	4895 ± 214
3194	31	7.55	3	22.62 ± 0.36		22.62 ± 0.36	408 ± 11	8.21	928 ± 78	5106 ± 226
3194	31	7.55	3	22.05 ± 0.36		22.05 ± 0.36	419 ± 11	8.17	836 ± 78	4984 ± 218
3194	31	7.55	1	19.15 ± 0.39		19.15 ± 0.39	342 ± 11	7.92	605 ± 93	5888 ± 330
3194	31	7.55	2	22.07 ± 0.28	22.14 ± 0.28	22.10 ± 0.20	455 ± 11	8.17	773 ± 61	4585 ± 202

pCO_{2sw}, seawater pCO_2 of the culture treatment. *T*, seawater temperature of the culture treatment. pH_{sw}, seawater pH of the culture treatment. Tank, tank number where the sample was cultured. $\delta^{11}Bc_1$, first measurement of the boron isotopic composition of the sample, uncertainty determined on reproducibility of the AE121 standard (2 SD). $\delta^{11}Bc_2$, duplicate analysis of the boron isotopic composition of the sample, uncertainty determined on reproducibility of the AE121 standard (2 SD). $\delta^{11}B_{average}$, average of $\delta^{11}B_{c1}$ and $\delta^{11}B_{c2}$ or $\delta^{11}B_{c1}$ if only one measurement was performed. When two measurements were carried out uncertainty was calculated based on uncertainties of $\delta^{11}B_{c1}$: and $\delta^{11}B_{c2}$ ($\Delta a = \sqrt{(\Sigma i(\Delta ai)^2)}$). B/Ca measured for the sample. Uncertainty is based 2 SD on the reproducibility of the CamWuellestorfi (table S4). pH_{cf} calculated from $\delta^{11}B$ using (*8*) based on Monte Carlo simulation. $[CO_3^{2-}]_{cf}$ calculated from B/Ca using (*8*). DIC_{cf} calculated from $\delta^{11}B$ and B/Ca using (*8*). Uncertainties for $[CO_3^{2-}]$cf and DIC_{cf} calculated using (*8*), Δ (1 SE) = $\sqrt{(\Sigma i(\Delta sysi + \Delta nonsysi)^2)}$, ^{x}uncertainty = Δnonsys (1 SE). Additional data not used in this study (Li/Ca, Mg/Ca and Sr/Ca) are presented in table S7 in the Supplementary Materials.

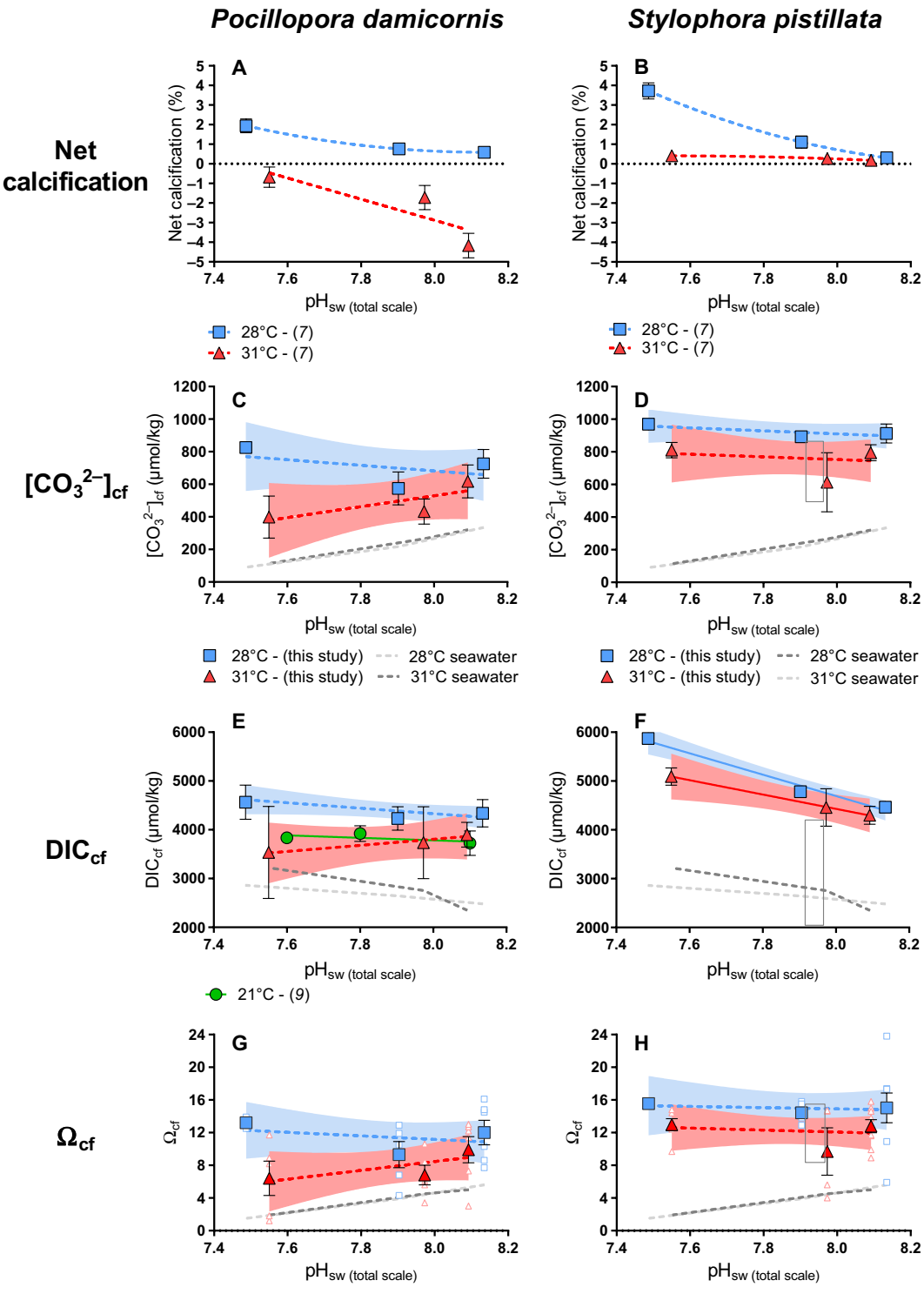

Fig. 2. Carbonate chemistry of the calcifying fluid–based boron proxies. Panels show measured parameters as a function of treatment pH_{sw}. Blue squares correspond to 28°C, red triangles correspond to 31°C, solid symbols represent treatment averages, and open symbols represent data for individual coral specimens. (**A**) and (**B**) show net calcification rate as percent change in skeletal mass throughout the experiment (*7*). (**C**) and (**D**) show recalculated $[CO_3^{2-}]_{cf}$. (**E**) and (**F**) show calculated DIC_{cf}. (**G**) and (**H**) show calculated saturation state of aragonite in the calcifying fluid (Ω_{cf}). Gray rectangles in (D), (F), and (H) represent the range (2 SD) of LIX data (*32*) for *S. pistillata* [pH 7.94 (total scale), $T = 25$°C, $S = 38$]. Best-fit model (linear or nonlinear regressions) was determined using GraphPad based on lowest AIC. Solid lines indicate significant regressions ($P < 0.05$). Dashed gray lines represent 1:1 ratio of $[CO_3^{2-}]_{cf}$:$[CO_3^{2-}]_{sw}$, DIC_{cf}:DIC_{sw}, or Ω_{cf}:Ω_{sw} for comparison to observed trends (28°C, dark; 31°C, light). Error bars are given in SEM and envelopes for the regressions represent 95% confidence interval.

The observed increases in DIC_{cf} cannot be solely explained by the prescribed increases in DIC_{sw} because the change in DIC_{cf} did not consistently track the change in DIC_{sw} ($\Delta DIC_{cf}/\Delta DIC_{sw}$). Neither can the hypothesis that DIC_{cf} increases under conditions of OA owing to decreased calcification rate [i.e., via accumulation of DIC in the calcifying fluid; (*6*)] explain the observed DIC_{cf} trends, since both DIC_{cf} and calcification rate increased with acidification. Instead, it appears that the changes in DIC_{cf} were the cause, rather than the result, of the changes in calcification rate resulting from the prescribed OA.

Ω_{cf}

The capacity of an organism to elevate aragonite saturation state at the site of calcification supports precipitation of its skeleton (*6*, *38*, *46*). Prior work has shown that $[Ca^{2+}]$ of the coral calcifying fluid ($[Ca^{2+}]_{cf}$) can differ from $[Ca^{2+}]$ of seawater ($[Ca^{2+}]_{sw}$) (Fig. 2, G and H), with $[Ca^{2+}]_{cf}/[Ca^{2+}]_{sw}$ of *P. damicornis* ranging from 0.85 to 1.41 (*32*, *60*) and *S. pistillata* exhibiting $[Ca^{2+}]_{cf}/[Ca^{2+}]_{sw}$ of 1.18 (*32*). Owing to the absence of direct measurements of $[Ca^{2+}]_{cf}$ in the present study, we conservatively used $[Ca^{2+}]$ of seawater but acknowledge that more accurate estimates of Ω_{cf} could be obtained from direct measurements of $[Ca^{2+}]_{cf}$ under the difference treatments. Although using a constant value of $[Ca^{2+}]_{cf}$ yields responses in $[CO_3^{2-}]_{cf}$ and Ω_{cf} that are of identical shape, estimation of Ω_{cf} is useful because it presents the carbonate chemistry of the calcifying fluid relative to the nonarbitrary chemical division between the precipitation and dissolution of inorganic aragonite (i.e., $\Omega = 1$).

Ω_{cf} is significantly greater at 28°C than at 31°C for *S. pistillata* under all pCO_2 conditions (400 ppm, $P = 0.0002$; 1000 ppm, $P < 0.0001$; 2800 ppm, $P < 0.0001$) and for *P. damicornis* under a pCO_2 of 2800 ppm ($P = 0.03$). Both species maintained $\Omega_{cf} \geq 5$ under all treatments, well above the level favoring dissolution of inorganic aragonite ($\Omega_{cf} < 1$). Under the control (optimal) temperature treatments, Ω_{cf} was elevated as high as 16—a level that supports spontaneous precipitation of aragonite from seawater (*61*). Yet, despite maintaining Ω_{cf} that is elevated relative to Ω_{sw} by 2 to 4 units under thermal stress (31°C), the rate of gross calcification for *P. damicornis* was less than its rate of gross dissolution, which caused the corals to exhibit net dissolution under all pCO_2 conditions at 31°C.

These estimates of Ω_{cf} are consistent with the results of recent studies that used microsensors and fluorescent dyes (*32*), boron geochemistry (*9*), and Raman spectroscopy (*60*) to characterize calcifying fluid chemistry in the same species. Our observations of thermally induced declines in Ω_{cf} are also in line with recent studies on the calcifying fluid dynamics of *Porites* corals in nature settings (*10*, *43*, *46*, *47*). However, our results are not consistent with the finding of Comeau *et al.* (*9*) that Ω_{cf} decreased with pH_{cf} by ca. 3 units of Ω_{cf} over 0.2 pH_{sw} units. Instead, we found that Ω_{cf} of both species remained constant with decreasing pH_{sw} (for *P. damicornis* at 28°C: ANOVA, $P = 0.19$ and at 31°C: ANOVA, $P = 0.28$; for *S. pistillata* at 28°C: ANOVA, $P = 0.90$ and at 31°C: ANOVA, $P = 0.51$).

Fidelity of coral skeletal $\delta^{11}B$ in recording coral pH_{cf}

The skeletal $\delta^{11}B$ composition of corals has been widely used as a proxy for pH_{cf} [e.g., (*9*, *10*, *57*), among others]. However, few studies have independently measured pH_{cf} to assess the reliability of the $\delta^{11}B$ proxy of pH_{cf} in corals (*39*), and none have done this with the pH microelectrode approach (Fig. 4). Holcomb *et al.* (*62*) found that the pH-sensitive dye (SNARF) and skeletal boron isotope approaches yielded different estimates of pH_{cf} for *S. pistillata*, which they attributed to the two approaches analyzing different portions of the coral skeleton. Sevilgen *et al.* (*32*) found that the microelectrode and SNARF approaches yielded statistically indistinguishable estimates of pH_{cf}, although they reported that the microelectrode approach yielded greater variability—possibly due to polyp retraction, stress response, and/or fluid mixing during microelectrode insertion.

In this study, pH_{cf} was independently measured with proton-sensitive microelectrodes (*7*) in the same coral specimens that were measured for skeletal $\delta^{11}B$, allowing direct comparison of $\delta^{11}B$-derived pH_{cf} and microelectrode-derived pH_{cf}. The microelectrode pH_{cf} measurements were performed in both the light (pH_{cf_light}) and dark (pH_{cf_dark}) (Figs. 1, E and F, 5, and 6; Table 4; and table S2). The $\delta^{11}B$-based estimates of pH_{cf} are significantly correlated with the microelectrode-based pH_{cf} measurements for both species (Fig. 5, A and B). As discussed in the "pH_{cf}" section, pH_{cf} derived from both the $\delta^{11}B$ and the microelectrode approaches show the same response to temperature (i.e., decreasing pH_{cf} under thermal stress) and to pH_{sw}. However, the microelectrode estimate of pH_{cf_light} and pH_{cf_dark} are, in some cases, significantly different from the $\delta^{11}B$ estimates of pH_{cf} in absolute magnitude. For *S. pistillata*, the difference between microelectrode pH_{cf_light} and $\delta^{11}B$ pH_{cf} is greatest and statistically

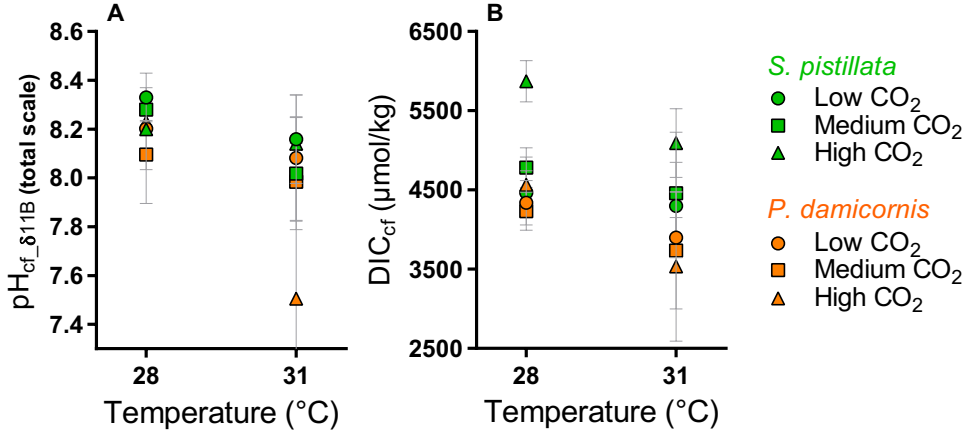

Fig. 3. Effect of temperature on the carbonate chemistry of the calcifying fluid in this study. Effect of temperature on $pH_{cf\_\delta11B}$ (**A**) and DIC_{cf} (**B**) of *S. pistillata* (green) and *P. damicornis* (orange). Error bars are given as SEM.

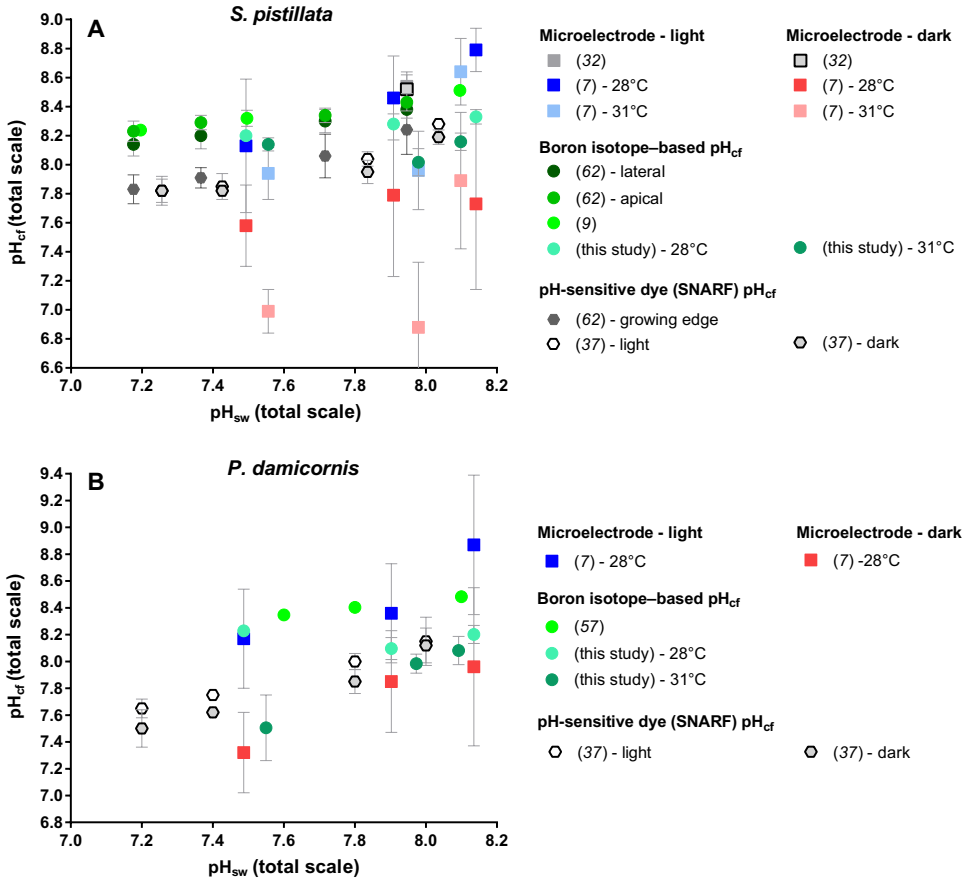

Fig. 4. Compilation of pH_{cf} under OA from direct and indirect measurements for *S. pistillata* and *P. damicornis*. Compilation of existing pH_{cf} data from microelectrode, pH-sensitive-dye (SNARF), and boron isotope data. (**A**) *S. pistillata*. (**B**) *P. damicornis*. Error bars are given in SD.

significant at pH_{sw} 8.1 (28°C, $P = 0.01$; 31°C, $P = 0.02$). At lower pH_{sw}, pH_{cf_light} and $\delta^{11}B$ estimates of pH_{cf} were not significantly different ($P > 0.05$) (Figs. 1 and 6). In contrast, pH_{cf_dark} was significantly different from $\delta^{11}B$ estimates of pH_{cf} under the lowest pH treatment for both species and at both temperatures (*P. damicornis* at 28°C, $P = 0.03$; *S. pistillata* at 28°C, $P = 0.02$; *S. pistillata* at 31°C, $P < 0.0001$).

Both species exhibited an increase in pH_{cf} in the light relative to the dark under all treatments, most likely owing to photosynthetic drawdown of DIC leading to elevated solution pH_{sw}—a phenomenon previously observed in zooxanthellate corals by Al-Horani *et al.* (*40*). Average pH_{cf} derived from $\delta^{11}B$ consistently fell between the averages of pH_{cf_light} (e.g., higher than $\delta^{11}B$ estimates of pH_{cf}) and pH_{cf_dark} (e.g., lower than $\delta^{11}B$ estimates of pH_{cf}). These findings support the assertion that $\delta^{11}B$ is reflecting time-averaged pH_{cf} (possibly diurnal), while microelectrode pH_{cf} captures instantaneous pH_{cf} under whatever irradiance conditions exist at the time of measurement (light or dark). Thus, the discrepancy between these two approaches to estimating pH_{cf} may arise from the fact that the microelectrode approach measures instantaneous pH_{cf} at the particular time that the microelectrode is inserted, while $\delta^{11}B$ reflects a time-averaged pH_{cf}.

It is also possible that the $\delta^{11}B$ and microelectrode measurements are slightly offset because of differing analytical errors and/or the possibility that the two approaches are sampling slightly different regions of the calcifying fluid. However, the fact that both techniques capture the same general trends in pH_{cf} in response to both pH_{sw} and thermal stress suggests that the observed trends are reliable.

The comparison of both approaches to measuring pH_{cf} yields unique insight into the mechanism of coral biomineralization. One hypothesis arising from the observation in both species is that $\delta^{11}B$-based estimates of pH_{cf} at 28°C are more similar to pH_{cf_dark} than to pH_{cf_light} at the lowest pCO_2 treatment and that symbiont photosynthesis is DIC-limited under low CO_2/high pH_{sw} conditions, potentially shifting the timing of rapid calcification away from the time of peak photosynthesis when DIC_{cf} is lowest. Conversely, $\delta^{11}B$ pH_{cf} may be more similar to pH_{cf_light} under higher pCO_2 treatments because DIC may no longer be limiting for symbiont photosynthesis under these conditions, meaning that maximum calcification can proceed coevally with maximum photosynthesis without competing for DIC.

CO_2-induced fertilization of symbiont photosynthesis links OA to observed trends in coral calcification rate and calcifying fluid chemistry

The mechanism linking the prescribed OA to the observed trends in DIC_{cf}, pH_{cf}, Ω_{cf}, and calcification rate may be the CO_2-induced fertilization of photosynthesis by the coral's algal symbionts [e.g., (*55*, *56*)]. Under conditions of OA, the photosynthetic activity of the coral's algal symbionts increases [e.g., (*3*, *57*, *63*, *64*)] up to the point that CO_2 is no longer limiting for the algae. This should increase the energy available to the coral host for physiological processes, including maintenance of the elevated pH_{cf} with respect to acidified seawater via proton pumping [through increased production

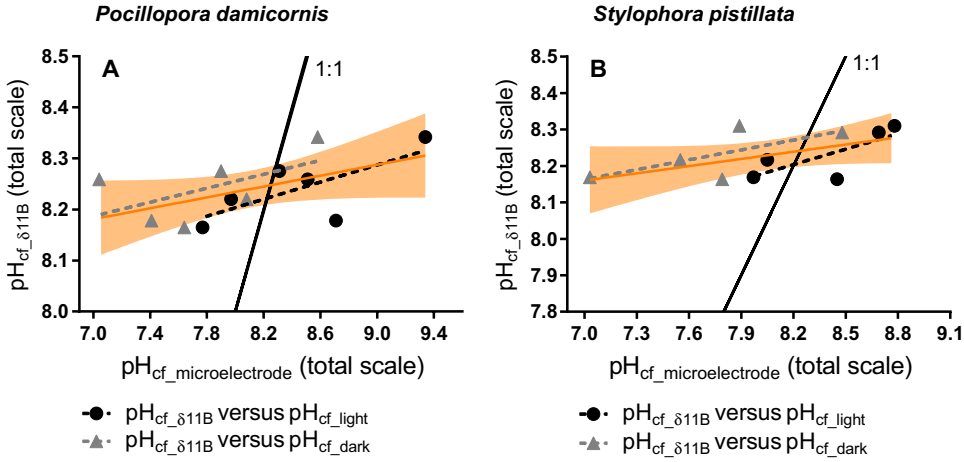

Fig. 5. Comparison between pH_{cf} from skeletal $\delta^{11}B$ and direct LIX measurements. Comparison of pH_{cf} from skeletal $\delta^{11}B$ ($pH_{cf\_\delta11B}$) and pH_{cf} from microelectrode measurements (*7*) in the light (pH_{cf_light}, black dots) and in the dark (pH_{cf_dark}, gray triangles) for individual coral specimens of *P. damicornis* (**A**) and for *S. pistillata* (**B**) measured in the same samples. LRs of pH_{cf_light} (dashed black line), pH_{cf_dark} (dashed gray line), and both pH_{cf}-based microelectrode (orange line) versus $pH_{cf\_\delta11B}$. The black line represents 1:1 ratio of $pH_{cf\_\delta11B}$:$pH_{cf\_microelectrode}$ for comparison to observed trends. The orange line is the LR between pH_{cf} from $\delta^{11}B$ and pH_{cf} derived from microelectrode (both light and dark), and the orange envelop represents the 95% confidence interval for LR.

of adenosine 5′-triphosphate (ATP)], while simultaneously increasing the coral's metabolic supply of DIC to its calcifying fluid (via increased respiration of translocated photosynthate)—which are both supportive of calcification by increasing Ω_{cf}. Increased DIC in the external seawater under high CO_2 may also propagate directly into the coral calcifying fluid, contributing to the higher DIC_{cf} observed in the present study.

The CO_2-induced fertilization of symbiont photosynthesis seems to be the most parsimonious mechanism to explain the observed link between the prescribed CO_2-induced acidification and the resulting increase in DIC_{cf}, stable pH_{cf}, and Ω_{cf}, and positive net calcification rate. The one treatment for which these relationships were not observed was *P. damicornis* at 31°C, for which pH_{cf} declined and DIC_{cf} remained constant with decreasing pH_{sw}, and net calcification rate was negative (i.e., net dissolution) under all pCO_2 treatments. *P. damicornis* specimens exhibited severe bleaching under these conditions—up to 60% more than *S. pistillata* at 31°C. This increased bleaching (i.e., reduction in symbiont density) would have severely limited the benefits arising from the CO_2-induced fertilization of symbiont photosynthesis, which may be at least partly responsible for the decline in pH_{cf} with decreasing pH_{sw} (i.e., in the absence of symbionts, the corals lacked the energy to control calcifying fluid chemistry) and the net dissolution exhibited by the *P. damicornis* specimens under all pCO_2 treatments at 31°C. Thus, when the symbionts were removed from the *P. damicornis* host via thermally induced bleaching, this species was no longer able to maintain constant pH_{cf} and Ω_{cf} across pCO_2 treatments, causing calcification rates to become negative (i.e., net dissolution). The impacts of the increased bleaching of *P. damicornis* relative to *S. pistillata* are also consistent with the increased offset in pH_{cf}, DIC_{cf}, and net calcification rate between the two temperature treatments (i.e., because of increased bleaching in the higher temperature treatments) at equivalent pCO_2 for *P. damicornis*, compared to *S. pistillata* (Figs. 1 to 3).

However, our hypothesis that CO_2-induced fertilization of photosynthesis is the cause of the trends observed in the present study is challenged by the lack of direct measurements of symbiont photosynthesis by reports of recent studies that elevated pCO_2 can have a null or even negative effects on symbiont photosynthesis (*4*, *65*). An additional and potentially complementary explanation for the observed trends is that environmental stress impairs coral calcification and control over calcifying chemistry by increasing paracellular permeability (leakiness), as recently observed by Venn *et al.* (*66*) for *S. pistillata* exposed to OA. Although increased paracellular permeability in corals has not yet been observed in response to thermal stress, the results of the present study suggest that thermal stress may exacerbate any increased paracellular permeability associated with OA.

The results of the present study suggest that some species of zooxanthellate corals are able to cope with the deleterious impacts of moderate OA by way of the increased energy acquired through CO_2-induced fertilization of their algal symbionts. However, once the coral-symbiont relationship breaks down as a result of thermally induced bleaching, *P. damicornis* appears to lose this built-in resilience to OA. These results are consistent with the assertion that thermally induced bleaching is the mechanism behind the strongly negative interaction between the impacts of thermal stress and OA on coral calcification. Although it is possible that these trends are driven by thermal impairment of enzymes used in calcification and/or photosynthesis, such as CA, the observation that *P. damicornis* exhibited greater bleaching than *S. pistillata* at 31°C and also exhibited calcifying fluid chemistry and calcification rates that were more negatively affected than those of *S. pistillata* (Figs. 1 and 3) suggests that thermally induced bleaching is the primary driver behind the negative interaction between thermal stress and OA on coral calcification.

Implications for models of scleractinian coral calcification

Mechanisms of coral biomineralization have been interrogated with a wide array of approaches, including isotopic and elemental geochemistry of the coral skeleton (*9*), cellular biological approaches, histology, ion-sensitive microelectrodes and dyes, and physical/mathematical modeling (*7*, *24*, *39*, *40*). Many of these studies address the role that pH_{sw} and carbonate chemistry of the calcifying fluid play in coral biomineralization, while others address the roles that organic molecules and tissues play in the nucleation and growth

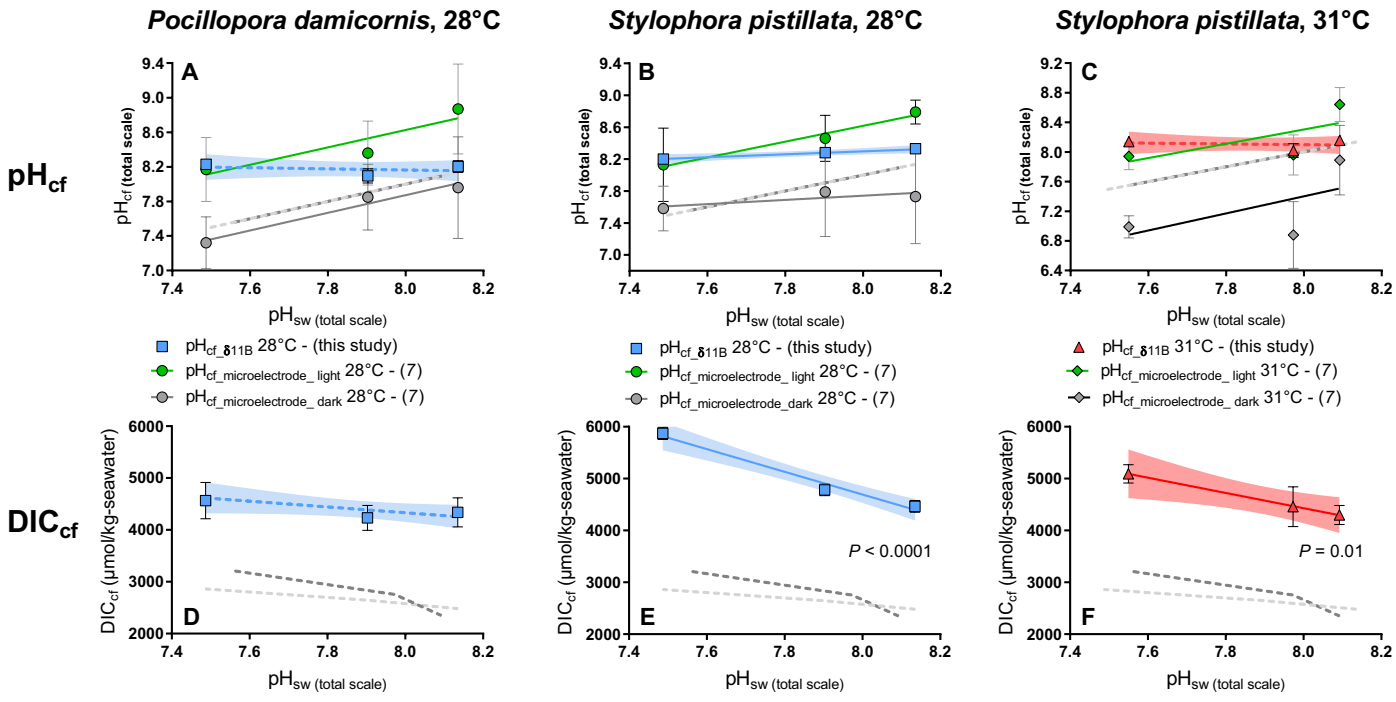

Fig. 6. pH_{cf} and DIC_{cf} from boron proxies and pH_{cf} from LIX measurements. (**A** to **C**) Comparison between averages of boron-based pH_{cf} (blue or red symbols) and microelectrode-derived pH_{cf} in the light (open symbols) and in the dark (solid gray symbols) at the two temperature treatments for *P. damicornis* [(A) 28°C; no microelectrode pH_{cf} data at 31°C] and *S. pistillata* [(B) 28°C and (C) 31°C]. LRs of pH_{cf_light} (orange, 28°C; green, 31°C), pH_{cf_dark} (black, 28°C; gray, 31°C), and $pH_{cf\_\delta11B}$ (blue, 28°C; red, 31°C) versus pH treatment. (**D** to **F**) DIC_{cf} data calculated from B/Ca and δ^{11}B-derived pH_{cf} for *P. damicornis* [(D) 28°C; no microelectrode pH data at 31°C] and *S. pistillata* [(E) 28°C and (F) 31°C]. Dashed gray lines represent 1:1 ratio of pH_{cf}:pH_{sw} for comparison to observed trends (28°C, dark; 31°C, light). Error bars are given in SEM and envelopes for the regressions represent 95% confidence interval.

of the aragonite crystals that comprise the coral skeleton (*20*, *22*, *67*). Compensatory responses to OA involve not only pH_{cf} regulation but also differential expression of genes and proteins involved in biomineralization, including enzymes such as CA [e.g., (*21*)].

Studies differ in the emphasis placed on the roles that regulation of calcification site pH_{cf} and carbonate chemistry play in the coral calcification response to environmental change. We use two independent recorders of pH_{cf}: the microelectrode approach that records instantaneous pH_{cf} in the bulk calcifying fluid and skeletal boron geochemistry (δ^{11}B and B/Ca) that records a time-integrated signal of pH_{cf} and carbonate chemistry at the site of crystal formation. These two techniques both reveal a loss of control over coral pH_{cf} under thermal stress and yield estimates of pH_{cf} that are elevated relative to pH_{sw} and intracellular pH. Differences in absolute pH_{cf} estimates between the microelectrode and δ^{11}B techniques under controlled experimental conditions may be most easily explained as reflecting differences in the time scales that these techniques record pH_{cf}, but these differences may also reflect processes of coral biomineralization that are not yet fully constrained, such as maintenance of pH gradients within the calcifying fluid. The boron geochemical and microelectrode data agree that the coral species studied exert less control over pH_{cf} under thermal stress and that this loss of control over calcifying fluid chemistry is strongly associated with decreased rate calcification. These results identify a previously unreported mechanism by which thermal and acidification stressors interact to impair scleractinian coral calcification (i.e., thermal stress reduces coral control over calcifying fluid carbonate chemistry, compromising coral ability to mitigate impacts of acidification) and confirm the role that coral control over calcifying fluid chemistry plays in the coral calcification response to OA.

The following conclusions can be drawn from the present study:

1) Specimens of *P. damicornis* and *S. pistillata* exhibit stable or increasing pH_{cf}, DIC_{cf}, Ω_{cf}, and net calcification with decreasing pH_{sw} under the corals' optimal temperature conditions (28°C). However, under conditions of thermal stress (31°C), *P. damicornis* (but not *S. pistillata*) exhibits an inversion of these trends—i.e., decreasing pH_{cf} and DIC_{cf} with decreasing pH_{sw} combined with net skeletal dissolution under all pH_{sw} treatments. The observation that *P. damicornis* also exhibited more intense bleaching under the high-temperature treatment than *S. pistillata* suggests that the coral's loss of symbionts caused the observed inversion of these trends—lowering its resilience to OA.

2) Specimens of *P. damicornis* and *S. pistillata* exhibited significant decreases in pH_{cf}, DIC_{cf}, and Ω_{cf} in response to thermal stress, when pCO_2 was held constant. These are the first controlled laboratory experiments to reveal that thermal stress, in addition to OA, renders the coral calcifying fluid less supportive of calcification.

3) Collectively, these results suggest that corals that retain their symbionts are able to cope with moderate OA via CO_2-induced fertilization of photosynthesis, which should increase the energy available to the coral host for pH_{cf} elevation via proton pumping (via increased production of ATP), while simultaneously increasing the coral's metabolic supply of DIC to its calcifying fluid (via increased respiration of translocated photosynthate), which leads to stable or increased Ω_{cf} and positive rates of calcification. These results are consistent with the assertion that thermally induced bleaching is the

Table 4. Measurements of pH_{cf} from microelectrode in the light (pH_{cf_light}) and dark (pH_{cf_dark}), $pH_{cf\_\delta 11B}$ calculated from skeletal $\delta^{11}B$, and estimated light:dark calcification ratios.

	pH_{cf_light} (±SE) (total scale)	pH_{cf_dark} (±SE) (total scale)	$\Delta pH_{light\text{-}dark}$ (±SE) (total scale)	$pH_{cf\_\delta 11B}$ (±SE) (total scale)	Light:dark calcification
P. damicornis					
pCO_2 466 ppm, 28°C	8.93 ± 0.30	8.03 ± 0.34	0.9 ± 0.5	8.20 ± 0.07	19:81
pCO_2 925 ppm, 28°C	8.43 ± 0.22	7.92 ± 0.22	0.5 ± 0.3	8.10 ± 0.08	35:65
pCO_2 2807 ppm, 28°C	8.24 ± 0.22	7.39 ± 0.17	0.9 ± 0.3	8.23 ± 0.02	99:01
S. pistillata					
pCO_2 466 ppm, 28°C	8.86 ± 0.07	7.80 ± 0.30	1.1 ± 0.6	8.29 ± 0.12	50:50
pCO_2 925 ppm, 28°C	8.53 ± 0.15	7.86 ± 0.28	0.6 ± 0.3	8.28 ± 0.02	63:37
pCO_2 2807 ppm, 28°C	8.20 ± 0.23	7.65 ± 0.14	0.6 ± 0.3	8.20 ± 0.01	100:00*
pCO_2 499 ppm, 31°C	8.71 ± 0.12	7.96 ± 0.24	0.9 ± 0.3	8.16 ± 0.05	27:73
pCO_2 885 ppm, 31°C	8.03 ± 0.14	6.95 ± 0.23	0.9 ± 0.3	8.04 ± 0.10	99:01
pCO_2 3194 ppm, 31°C	8.01 ± 0.09	7.06 ± 0.08	0.9 ± 0.1	8.14 ± 0.11	100:00*

pH_{cf_light}, pH_{cf} measured from microelectrode when the coral was in the light; uncertainty is reported as 1 SE of the replicates. pH_{cf_dark}, pH_{cf} measured from microelectrode when the coral was in the dark; uncertainty is reported as 1 SE of the replicates. $\Delta pH_{light\text{-}dark}$, difference in light and dark pH_{cf} microelectrode measurements $pH_{cf\_diurnal}$: pH_{cf} calculated from $\delta^{11}B$; uncertainty is reported as 1 SE of the replicates. Light:dark calcification, light:dark calcification ratios obtained from the weighting of pH_{cf_light} and pH_{cf_dark} measurements required to generate the $\delta^{11}B$-based estimates of pH_{cf} ($pH_{cf\_\delta 11B}$) calculated from average of measured specimens within a treatment. *When $pH_{cf\_diurnal}$ average was > or = pH_{cf_light} but still within errors of each other, we attributed a light:dark calcification of 100:00.

mechanism behind the strongly negative interaction between the impacts of thermal stress and OA on coral calcification.

4) A novel comparison of the $\delta^{11}B$-based and microelectrode-based approaches to measuring pH_{cf} reveal that these measurements are correlated but that $\delta^{11}B$ estimates are consistently offset from the microelectrode estimates of pH_{cf}. This may be explained by the fact that the microelectrode approach measures pH_{cf} at an instant in time—i.e., under whatever light condition was deployed at the time of microelectrode deployment—while the $\delta^{11}B$ approach records a time-integrated estimate of pH_{cf} that may represent an average of light and dark pH_{cf}. Nevertheless, both techniques support the assertions that corals elevate pH_{cf} relative to pH_{sw} under ambient and elevated pCO_2 and exhibit less control over pH_{cf} under thermal stress.

5) Correlation between coral control over calcifying fluid chemistry and net calcification responses to warming and acidification reaffirms the importance of calcifying fluid chemistry in the response of scleractinian corals to global change stressors.

MATERIALS AND METHODS

Experimental design

P. damicornis and *S. pistillata* are pocilloporid corals that host zooxanthellae dinoflagellates of the family *Symbiodiniaceae* (*68*). Specimens of *P. damicornis* and *S. pistillata* were obtained from De Jong Marinelife and originally collected from multiple colonies in the Fiji Islands. Seasonal temperatures in the Fiji Islands range from 25° to 29°C, with an annual average temperature of 27°C, a pCO_2 of 360 ppmv (parts per million volume), and a pH_{sw} of 8.08 (*69*). Experiments used three pCO_2 regimes (466/499 ppm, 925/885 ppm, and 2807/3194 ppm) crossed with two temperatures (28° and 31°C), yielding six treatments in total that were each replicated in four independent tanks. Although it is unlikely that coral reefs will experience pCO_2 levels as high as the highest pCO_2 treatments used in the present study, these treatments were used to elicit a strong response in the corals to elucidate the physiological mechanism(s) underlying corals' response to OA.

Natural seawater, originally collected from Spitsbergen, Norway, was continuously added to the experimental flow-through aquarium system at a rate of 0.6 liters/hour to prevent material depletion of alkalinity, $[Ca^{2+}]$, or other seawater constituents throughout the duration of the study. Aquaria were illuminated at 150 lux with actinic blue and white lights on a 12-hour on/off cycle. Fragments of both species (*S. pistillata* = 65 and *P. damicornis* = 63) were mounted onto eggcrate stands labeled with a unique identifier and split evenly among experimental treatments. Corals were fed 1-day-old *Artemia salina* nauplii hatched from ~40 mg of eggs. Ten milliliters of concentrated live nauplii was introduced to each replicate tank every second day. Ten-liter replicate acrylic tanks were fed by 244-liter recirculating sumps containing protein skimmers, mechanical filters, and activated charcoal filters.

The experiment was conducted over an 8-week interval, which was preceded by 3 weeks of acclimation to laboratory and experimental conditions. The corals were maintained at control conditions during the first week of the acclimation, were exposed to gradually increasing pCO_2 and temperature until reaching target conditions during the second week, and were maintained at target conditions during the final week. Coral skeletons were marked with 3.2 g/liter-seawater calcein dye for 5 days before initial buoyant weighing to facilitate identification and extraction of new skeletal material that was produced exclusively under the experimental conditions. The calcein marker was imaged with a Nikon AZ100 stereomicroscope with a Nikon 96320 fluorescence filter cube. Measurements of pH_{cf} were performed with pH-sensitive

liquid-ion-exchanger (LIX) microsensors after 30 days of exposure to experimental conditions. As with any controlled laboratory experiment on corals, it is possible that the duration of exposure influenced the results, as corals may function normally over short time frames, but exhibit impaired function over longer time frames, or vice versa.

Seawater chemistry manipulation and measurement

The pCO_2 of the experimental tanks was maintained by vigorously bubbling mixtures of CO_2-free air and CO_2 into the 244-liter treatment sumps with microporous sparging tubes. The pCO_2 of the bubbled gases was achieved by mixing compressed CO_2-free air and compressed CO_2 with solenoid-valve mass flow controllers at flow rates proportional to the target pCO_2 conditions. Temperature (±SE) was maintained at 28 (±0.02)°C and 31 (±0.06)°C using 125-W aquarium heaters (EHEIM) controlled with a programmable thermostat.

Temperature, pH, and salinity of all replicate tanks were measured three times per week using a multielectrode probe (WTW Multi 3430 Set K). The pH electrode was calibrated before use at each treatment temperature with pH 4.00 and 7.00 National Bureau of Standards (NBS) buffers. The conductivity (salinity) probe was calibrated at each treatment temperature with certified seawater reference material of 33.347 salinity (Dickson CRM batch #154). Samples for the analysis of DIC and total alkalinity (TA) were collected weekly at midday. Samples for the analysis of DIC and TA were collected in 25-ml borosilicate glass vials sealed with rubber septae and in 50-ml polypropylene centrifuge tubes, respectively. After collection, DIC and TA samples were poisoned with 10 and 20 μM, respectively, of saturated $HgCl_2$ solution and refrigerated until analysis. TA was determined by open-cell potentiometric Gran titration (precision, 10 μmol/kg) and DIC was determined by coulometry using a Shimadzu DIC analyzer (precision, 10 μmol/kg), with both analytical systems calibrated with certified seawater reference material (Dickson CRM batch #154). pH_{sw} (total scale) was calculated on the basis of direct measurements of pH (NBS); results fell within 0.1 pH unit of pH_{sw} calculated from TA and DIC. Seawater pCO_2, carbonate ion concentration ($[CO_3^{2-}]$), bicarbonate ion concentration ($[HCO_3^-]$), aqueous CO_2, and aragonite saturation state (Ω) were calculated from measured TA and DIC with the program CO_2SYS, using Roy *et al.* (*70*) values for the K_1 and K_2 carbonic acid constants, the Mucci (*71*) value for the stoichiometric aragonite solubility product, and an atmospheric pressure of 1.015 atm (Table 1).

Seawater chemistry data are summarized in Tables 1 to 3, table S5, Figs. 1 and 2, and figs. S4 and S5. All data presented in those plots were tested for outliers using an extreme studentized deviate method in GraphPad software (*72*).

Microelectrode pH_{cf} measurements and calcification rate

pH_{cf} of the corals was measured with proton-sensitive LIX microelectrodes using the technique described in (*7*, *73*) (see the Supplementary Materials).

Measurement of coral calcification rate

Calcification rates were obtained using the buoyant weight technique (*74*) (see the Supplementary Materials).

Geochemical analyses

Sample cleaning was performed following Guillermic *et al.* (*75*). A double oxidative step was performed using H_2O_2 because of high organic matter of the coral skeletal samples. A weak acid leach was also performed using 0.001 N HCl. Boron was purified via microdistillation (*75*). Boron isotope analyses were carried out on a Thermo Fisher Scientific Neptune Plus multicollector inductively coupled plasma mass spectrometry (MC-ICPMS) at the University of Cambridge maintained at 10^{13} ohm resistance. Seawater samples were prepared using column chemistry and analyzed at the Pôle Spectrométrie Océan (PSO), Plouzané.

The B concentration of skeletal samples analyzed for $\delta^{11}B$ ranged from 10 parts per billion (ppb) B (~5 ng B) to 20 ppb B (~10 ng B) samples. Sensitivity was 8 mV/ppb B (e.g., 80 mV for 10 ppb B) in wet plasma at a sample aspiration rate of 50 μl/min. Procedural boron blanks ranged from 15 to 65 pg B (contributing less than 1% of the sample signal). The ^{11}B of the acid blank was measured at 1 mV, contributing less than 1% of the sample signal. No memory effect was observed within or across sessions. External reproducibility was ensured by repeated measurements of carbonate standard [JCP-1 (*76*) and NEP, see the Supplementary Materials] microdistilled at the same time as the samples. The $\delta^{11}B$ composition of the NEP standard ($\delta^{11}B_{NEP}$) was measured at 25.71 ± 0.79 per mil (‰) (2 SD, $n = 22$) over eight analytical sessions, with each number representing an ab initio processed sample from the present study, which are within error of the published value for the standard of 25.80 ± 0.89‰ (*35*). The $\delta^{11}B$ composition of the JCP-1 standard was measured at 24.06 ± 0.19‰ (2 SD, $n = 6$) over six analytical sessions, with each number representing an ab initio processed sample from the present study, which was within error of the published values of 24.37 ± 0.32‰ (*77*) and 24.42 ± 0.28‰ (table S3) (*35*).

The $\delta^{11}B$ analyses for *S. pistillata* were also measured independently at the Alfred Wegener Institute for Polar Studies (AWI) in Bremerhaven, Germany. Boron in the dissolved samples was separated from the matrix using the microdistillation technique and analyzed at a B concentration of ~3 to 4 ppb with a Nu Plasma II MC-ICPMS using secondary electron multipliers (SEMs), where high-mass ion counter 5 (IC5) was used for ^{11}B and IC0 for ^{10}B. Sample measurements were bracketed by NBS951 measurements and accompanied by regular analyses of the control standard AE121 ($\delta^{11}B$ = 19.82 ± 0.3‰).

Elemental ratio measurements

Elemental ratios were measured on a Thermo Fisher Scientific Element XR HR-ICP-MS at the PSO, Ifremer (Plouzané, France) after Ca analyses on an ICP-AES Ultima 2 *HORIBA* at the PSO (Plouzané, France) (*75*). Data quality and external reproducibility were maintained by the repeated measurement of an internal consistency standard "CamWuellestorfi" [courtesy of the University of Cambridge (*78*)].

Typical measured concentrations of procedural blanks for the trace element analyses for sessions in which samples were diluted to 30 ppm Ca were ^7Li < 3%, ^{11}B < 4%, ^{25}Mg < 0.1%, ^{87}Sr < 0.1%, and ^{43}Ca < 0.1%. Typical measured concentrations of blanks for the trace element analyses for sessions in which samples were diluted to 10 ppm Ca were ^7Li < 5%, ^{11}B < 6%, ^{25}Mg < 0.3%, ^{87}Sr < 2%, and ^{43}Ca < 0.1%. External reproducibility was quantified via repeated measurement of the consistency standard CamWuellestorfi (table S4). The X/Ca elemental ratio measurements of the external standard CamWuellestorfi were always within error of published values (table S4) (*78*). Analytical uncertainty of a single measurement was calculated from the repeated measurement of the CamWuellestorfi standard within a given analytical session. The analytical uncertainties

on the X/Ca elemental ratios are 0.6 µmol/mol for Li/Ca, 11 µmol/mol for B/Ca, 0.09 mmol/mol for Mg/Ca, and 0.01 mmol/mol for Sr/Ca (2 SD, $n = 39$).

Calculations of pH_{cf}, $[CO_3^{2-}]_{cf}$, and DIC_{cf}

The pH_{cf} was calculated from measurements of coral skeletal $\delta^{11}B$ following Hemming and Hanson (*29*)

$$pH_{ch} = pKB^* - \log\left(\frac{\delta^{11}Bsw - \delta^{11}B_c}{\delta^{11}Bsw - \alpha * \delta^{11}B_c - \varepsilon}\right) \quad (5)$$

with $pK_B^*(T, S)$ representing the dissociation constant, $\delta^{11}B_{sw}$ representing the boron isotopic composition of the culture seawater (measured), $\delta^{11}B_c$ representing the boron isotopic composition of the coral skeleton, and ε representing the boron isotopic fractionation between boric acid and borate ion [27.2‰ (*79*)].

The $[CO_3^{2-}]_{cf}$ was calculated from coral skeletal B/Ca and a partition coefficient (K_D) of 0.00297*exp(−0.0202*[H^+]) following McCulloch *et al.* (*10*); other partition coefficients were used and are presented in table S1. The DIC and $[CO_3^{2-}]$ were calculated using the MATLAB code provided in DeCarlo *et al.* (*8*), modified for various values of $\delta^{11}B_{sw}$. The aragonite saturation state from the calcifying fluid (Ω_{cf}, Eq. 3) was calculated using $[CO_3^{2-}]_{cf}$, $[Ca^{2+}] = 10.5$ mmol at 28°C, and 10.3 mmol at 31°C [based on results from (*46*) on a *Porites* coral]. K^*_{sp} is the stoichiometric solubility product for aragonite, which varies with temperature and salinity.

SUPPLEMENTARY MATERIALS

Supplementary material for this article is available at http://advances.sciencemag.org/cgi/content/full/7/2/eaba9958/DC1

REFERENCES AND NOTES

1. T. P. Hughes, K. D. Anderson, S. R. Connolly, S. F. Heron, J. T. Kerry, J. M. Lough, A. H. Baird, J. K. Baum, M. L. Berumen, T. C. Bridge, D. C. Claar, C. M. Eakin, J. P. Gilmour, N. A. J. Graham, H. Harrison, J. P. A. Hobbs, A. S. Hoey, M. Hoogenboom, R. J. Lowe, M. T. McCulloch, J. M. Pandolfi, M. Pratchett, V. G. Schoepf, Torda, S. K. Wilson, Spatial and temporal patterns of mass bleaching of corals in the Anthropocene. *Science* **359**, 80–83 (2018).
2. A. C. Baker, P. W. Glynn, B. Riegl, Climate change and coral reef bleaching: An ecological assessment of long-term impacts, recovery trends and future outlook. *Estuar. Coast. Shelf Sci.* **80**, 435–471 (2008).
3. S. Reynaud, N. Leclercq, S. Romaine-Lioud, C. Ferrier-Pagés, J. Jaubert, J. P. Gattuso, Interacting effects of CO_2 partial pressure and temperature on photosynthesis and calcification in a scleractinian coral. *Glob. Chang. Biol.* **9**, 1660–1668 (2003).
4. K. R. N. Anthony, D. I. Kline, G. Diaz-Pulido, S. Dove, O. Hoegh-Guldberg, Ocean acidification causes bleaching and productivity loss in coral reef builders. *Proc. Natl. Acad. Sci. U.S.A.* **105**, 17442–17446 (2008).
5. R. Rodolfo-Metalpa, F. Houlbrèque, É. Tambutté, F. Boisson, C. Baggini, F. P. Patti, R. Jeffree, M. Fine, A. Foggo, J.-P. Gattuso, J. M. Hall-Spencer, Coral and mollusc resistance to ocean acidification adversely affected by warming. *Nat. Clim. Change* **1**, 308–312 (2011).
6. A. L. Cohen, T. A. McConnaughey, Geochemical perspectives on coral mineralization. *Rev. Mineral. Geochem.* **54**, 151–187 (2003).
7. L. P. Cameron, C. Reymond, J. Bijma, J. Büscher, D. De Beer, R. T. Eagle, Symbiont-assisted calcifying fluid pH elevation aids coral resilience to ocean acidification. *In review* (2020).
8. T. M. DeCarlo, M. Holcomb, M. T. McCulloch, Reviews and syntheses: Revisiting the boron systematics of aragonite and their application to coral calcification. *Biogeosciences* **15**, 2819–2834 (2018b).
9. S. Comeau, C. E. Cornwall, M. T. McCulloch, Decoupling between the response of coral calcifying fluid pH and calcification to ocean acidification. *Sci. Rep.* **7**, 7573 (2017a).
10. M. T. McCulloch, J. P. D'Olivo, J. Falter, M. Holcomb, J. A. Trotter, Coral calcification in a changing world and the interactive dynamics of pH and DIC upregulation. *Nat. Commun.* **8**, 15686 (2017).
11. *IPCC: Climate Change 2014—The Physical Science Basis*, Intergovernmental Panel on Climate Change, Ed., (Cambridge Univ. Press, 2014).
12. D. Allemand, C. Ferrier-Pagès, P. Furla, F. Houlbrèque, S. Puverel, S. Reynaud, É. Tambutté, S. Tambutté, D. Zoccola, Biomineralisation in reef-building corals: From molecular mechanisms to environmental control. *Comptes Rendus Palevol* **3**, 453–467 (2004).
13. J. Erez, The source of ions for biomineralization in foraminifera and their implications for paleoceanographic proxies. *Rev. Mineral. Geochemistry* **54**, 115–149 (2003).
14. J. B. Ries, A physicochemical framework for interpreting the biological calcification response to CO_2-induced ocean acidification. *Geochim. Cosmochim. Acta* **75**, 4053–4064 (2011).
15. T. A. McConnaughey, R. H. Falk, Calcium-proton exchange during algal calcification. *Biol. Bull.* **180**, 185–195 (1991).
16. P. Furla, I. Galgani, I. Durand, D. Allemand, Sources and mechanisms of inorganic carbon transport for coral calcification and photosynthesis. *J. Exp. Biol.* **203**, 3445–3457 (2000).
17. D. Zoccola, P. Ganot, A. Bertucci, N. Caminiti-Segonds, N. Techer, C. R. Voolstra, M. Aranda, E. Tambutté, D. Allemand, J. R. Casey, S. Tambutté, Bicarbonate transporters in corals point towards a key step in the evolution of cnidarian calcification. *Sci. Rep.* **5**, 9983 (2015).
18. A. Moya, S. Tambutté, A. Bertucci, E. Tambutté, S. Lotto, D. Vullo, C. T. Supuran, D. Allemand, D. Zoccola, Carbonic anhydrase in the scleractinian coral *Stylophora pistillata*: Characterization, localization, and role in biomineralization. *J. Biol. Chem.* **283**, 25475–25484 (2008).
19. N. Allison, I. Cohen, A. A. Finch, J. Erez, A. W. Tudhope, Corals concentrate dissolved inorganic carbon to facilitate calcification. *Nat. Commun.* **5**, 5741 (2014).
20. S. Von Euw, Q. Zhang, V. Manichev, N. Murali, J. Gross, L. C. Feldman, T. Gustafsson, C. Flach, R. Mendelsohn, P. G. Falkowski, Biological control of aragonite formation in stony corals. *Science* **356**, 933–938 (2017).
21. J. L. Drake, M. F. Schaller, T. Mass, L. Godfrey, A. Fu, R. M. Sherrell, Y. Rosenthal, P. G. Falkowski, Molecular and geochemical perspectives on the influence of CO_2 on calcification in coral cell cultures. *Limnol. Oceanogr.* **63**, 107–121 (2018).
22. T. Mass, A. J. Giuffre, C.-Y. Sun, C. A. Stifler, M. J. Frazier, M. Neder, N. Tamura, C. V. Stad, M. A. Marcus, P. U. P. A. Gilbert, Amorphous calcium carbonate particles form coral skeletons. *Proc. Natl. Acad. Sci. U.S.A.* **114**, E7670–E7678 (2017b).
23. A. Akiva, M. Neder, K. Kahil, R. Gavriel, I. Pinkas, G. Goobes, T. Mass, Minerals in the pre-settled coral *Stylophora pistillata* crystallize via protein and ion changes. *Nat. Commun.* **9**, 1880 (2018).
24. A. Venn, E. Tambutté, M. Holcomb, D. Allemand, S. Tambutté, Live tissue imaging shows reef corals elevate pH under their calcifying tissue relative to seawater. *PLOS ONE* **6**, e20013 (2011).
25. A. J. Giuffre, A. C. Gagnon, J. J. De Yoreo, P. M. Dove, Isotopic tracer evidence for the amorphous calcium carbonate to calcite transformation by dissolution–reprecipitation. *Geochim. Cosmochim. Acta* **165**, 407–417 (2015).
26. T. M. DeCarlo, Characterizing coral skeleton mineralogy with Raman spectroscopy. *Nat. Commun.* **9**, 5325 (2018).
27. A. Akiva, M. Neder, K. Kahil, R. Gavriel, I. Pinkas, G. Goobes, T. Mass, Reply to: Characterizing coral skeleton mineralogy with Raman spectroscopy. *Nat. Commun.* **9**, 5324 (2018).
28. D. Evans, P. B. Webb, K. Penkman, R. Kröger, N. Allison, The characteristics and biological relevance of inorganic amorphous calcium carbonate (ACC) precipitated from seawater. *Cryst. Growth Des.* **19**, 4300–4313 (2019).
29. N. G. Hemming, G. N. Hanson, Boron isotopic composition and concentration in modern marine carbonates. *Geochim. Cosmochim. Acta* **56**, 537–543 (1992).
30. V. Mavromatis, V. Montouillout, J. Noireaux, J. Gaillardet, J. Schott, Characterization of boron incorporation and speciation in calcite and aragonite from co-precipitation experiments under controlled pH, temperature and precipitation rate. *Geochim. Cosmochim. Acta* **150**, 299–313 (2015).
31. J. Noireaux, V. Mavromatis, J. Gaillardet, J. Schott, V. Montouillout, P. Louvat, C. Rollion-Bard, D. R. Neuville, Crystallographic control on the boron isotope paleo-pH proxy. *Earth Planet. Sci. Lett.* **430**, 398–407 (2015).
32. D. S. Sevilgen, A. A. Venn, M. Y. Hu, E. Tambutté, D. de Beer, V. Planas-Bielsa, S. Tambutté, Full in vivo characterization of carbonate chemistry at the site of calcification in corals. *Sci. Adv.* **5**, eaau7447 (2019).
33. M. Holcomb, T. M. DeCarlo, G. A. Gaetani, M. McCulloch, Factors affecting B/Ca ratios in synthetic aragonite. *Chem. Geol.* **437**, 67–76 (2016).
34. N. Allison, Reconstructing coral calcification fluid dissolved inorganic carbon chemistry from skeletal boron: An exploration of potential controls on coral aragonite B/Ca. *Heliyon* **3**, e00387 (2017).
35. J. N. Sutton, Y.-W. Liu, J. B. Ries, M. Guillermic, E. Ponzevera, R. A. Eagle, $\delta^{11}B$ as monitor of calcification site pH in divergent marine calcifying organisms. *Biogeosciences* **15**, 1447–1467 (2018).
36. Y. W. Liu, J. N. Sutton, J. B. Ries, R. A. Eagle, Regulation of calcification site pH is a polyphyletic but not always governing response to ocean acidification. *Sci. Adv.* **6**, eaax1314 (2020).
37. A. A. Venn, E. Tambutté, N. Caminiti-Segonds, N. Techer, D. Allemand, S. Tambutté, Effects of light and darkness on pH regulation in three coral species exposed to seawater acidification. *Sci. Rep.* **9**, 2201 (2019).

38. M. T. McCulloch, J. P. D'Olivo, J. Falter, L. Georgiou, M. Holcomb, P. Montagna, J. A. Trotter, Boron isotopic systematics in scleractinian corals and the role of pH up-regulation. *Boron Isotopes* , 145–162 (2018).
39. A. A. Venn, E. Tambutte, M. Holcomb, J. Laurent, D. Allemand, S. Tambutte, Impact of seawater acidification on pH at the tissue–skeleton interface and calcification in reef corals. *Proc. Natl. Acad. Sci. U.S.A.* **110**, 1634–1639 (2013).
40. F. A. Al-Horani, S. M. Al-Moghrabi, D. de Beer, The mechanism of calcification and its relation to photosynthesis and respiration in the scleractinian coral *Galaxea fascicularis*. *Mar. Biol.* **142**, 419–426 (2003).
41. W.-J. Cai, Y. Ma, B. M. Hopkinson, A. G. Grottoli, M. E. Warner, Q. Ding, X. Hu, X. Yuan, V. Schoepf, H. Xu, C. Han, T. F. Melman, K. D. Hoadley, D. T. Pettay, Y. Matsui, J. H. Baumann, S. Levas, Y. Ying, Y. Wang, Microelectrode characterization of coral daytime interior pH and carbonate chemistry. *Nat. Commun.* **7**, 11144 (2016).
42. S. Comeau, E. Tambutté, R. C. Carpenter, P. J. Edmunds, N. R. Evensen, D. Allemand, C. Ferrier-Pagès, S. Tambutté, A. A. Venn, Coral calcifying fluid pH is modulated by seawater carbonate chemistry not solely seawater pH. *Proc. R. Soc. B* **284**, 20161669 (2017b).
43. C. L. Ross, J. L. Falter, M. T. McCulloch, Active modulation of the calcifying fluid carbonate chemistry (δ^{11}B, B/Ca) and seasonally invariant coral calcification at sub-tropical limits. *Sci. Rep.* **7**, 13830 (2017).
44. P. W. Glynn, Coral reef bleaching: Ecological perspectives. *Coral Reefs* **12**, 1–17 (1993).
45. R. Berkelmans, J. K. Oliver, Large-scale bleaching of corals on the Great Barrier Reef. *Coral reefs* **18**, 55–60 (1999).
46. J. P. D'Olivo, M. T. McCulloch, Response of coral calcification and calcifying fluid composition to thermally induced bleaching stress. *Sci. Rep.* **7**, 2207 (2017).
47. J. P. D'Olivo, G. Ellwood, T. M. DeCarlo, M. T. McCulloch, Deconvolving the long-term impacts of ocean acidification and warming on coral biomineralisation. *Earth Planet. Sci. Lett.* **526**, 115785 (2019).
48. O. Hoegh-Guldberg, G. J. Smith, The effect of sudden changes in temperature, light and salinity on the population density and export of zooxanthellae from the reef corals *Stylophora pistillata* Esper and *Seriatopora hystrix* Dana. *J. Exp. Mar. Biol. Ecol.* **129**, 279–303 (1989).
49. C. B. Bove, J. B. Ries, S. W. Davies, I. T. Westfield, J. Umbanhowar, K. D. Castillo, Common Caribbean corals exhibit highly variable responses to future acidification and warming. *Proc. R. Soc. B.* **286**, 20182840 (2019).
50. Y. Loya, K. Sakai, K. Yamazato, Y. Nakano, H. Sambali, R. van Woesik, Coral bleaching: The winners and the losers. *Ecol. Lett.* **4**, 122–131 (2001).
51. J. P. Gattuso, D. Allemand, M. Frankignoulle, Photosynthesis and calcification at cellular, organismal and community levels in coral reefs: A review on interactions and control by carbonate chemistry. *Am. Zool.* **39**, 160–183 (1999).
52. N. J. Silbiger, G. Goodbody-Gringley, J. F. Bruno, H. M. Putnam, Comparative thermal performance of the reef-building coral *Orbicella franksi* at its latitudinal range limits. *Mar. Biol.* **166**, 126 (2019).
53. R. Rowan, Thermal adaptation in reef coral symbionts. *Nature* **430**, 742–742 (2004).
54. C. D. Clausen, A. A. Roth, Effect of temperature and temperature adaptation on calcification rate in the hermatypic coral *Pocillopora damicornis*. *Mar. Biol.* **33**, 93–100 (1975).
55. J. B. Ries, A. L. Cohen, D. C. McCorkle, Marine calcifiers exhibit mixed responses to CO_2-induced ocean acidification. *Geology* **37**, 1131–1134 (2009).
56. K. D. Castillo, J. B. Ries, J. F. Bruno, I. T. Westfield, The reef-building coral *Siderastrea siderea* exhibits parabolic responses to ocean acidification and warming. *Proc. R. Soc. B* **281**, 20141856 (2014).
57. S. Krief, E. J. Hendy, M. Fine, R. Yam, A. Meibom, G. L. Foster, A. Shemesh, Physiological and isotopic responses of scleractinian corals to ocean acidification. *Geochim. Cosmochim. Acta* **74**, 4988–5001 (2010).
58. R. H. McLachlan, J. T. Price, S. L. Solomon, A. G. Grottoli, Thirty years of coral heat-stress experiments: A review of methods. *Coral Reefs* **39**, 885–902 (2020).
59. S. Tambutté, E. Tambutté, D. Zoccola, D. Allemand, Organic matrix and biomineralization of scleractinian corals, in *Handbook of Biomineralization: Biological Aspects and Structure Formation* (Wiley, 2007), pp. 243–259.
60. T. M. DeCarlo, S. Comeau, C. E. Cornwall, M. T. McCulloch, Coral resistance to ocean acidification linked to increased calcium at the site of calcification. *Proc. R. Soc. B Biol. Sci.* **285**, 20180564 (2018a).
61. W. Sun, S. Jayaraman, W. Chen, K. A. Persson, G. Ceder, Nucleation of metastable aragonite $CaCO_3$ in seawater. *Proc. Natl. Acad. Sci. U.S.A.* **112**, 3199–3204 (2015).
62. M. Holcomb, A. A. Venn, E. Tambutté, S. Tambutté, D. Allemand, J. Trotter, M. McCulloch, Coral calcifying fluid pH dictates response to ocean acidification. *Sci. Rep.* **4**, 5207 (2014).
63. C. Langdon, M. J. Atkinson, Effect of elevated pCO_2 on photosynthesis and calcification of corals and interactions with seasonal change in temperature/ irradiance and nutrient enrichment. *J. Geophys. Res.* **110**, C09S07 (2005).
64. S. H. C. Noonan, K. E. Fabricius, Ocean acidification affects productivity but not the severity of thermal bleaching in some tropical corals. *ICES J. Mar. Sci.* **73**, 715–726 (2016).
65. C. B. Wall, T.-Y. Fan, P. J. Edmunds, Ocean acidification has no effect on thermal bleaching in the coral *Seriatopora caliendrum*. *Coral Reefs* **33**, 119–130 (2013).
66. A. A. Venn, C. Bernardet, A. Chabenat, E. Tambutté, S. Tambutté, Paracellular transport to the coral calcifying medium: Effects of environmental parameters. *J. Exp. Biol.* **223**, jeb227074 (2020).
67. S. Hohn, C. Reymond, Coral calcification, mucus, and the origin of skeletal organic molecules. *Coral Reefs* **38**, 973–984 (2019).
68. T. C. LaJeunesse, J. E. Parkinson, P. W. Gabrielson, H. J. Jeong, J. D. Reimer, C. R. Voolstra, S. R. Santos, Systematic revision of Symbiodiniaceae highlights the antiquity and diversity of coral endosymbionts. *Curr. Biol.* **28**, 2570–2580.e6 (2018).
69. R. M. Key, A. Kozyr, C. L. Sabine, K. Lee, R. Wanninkhof, J. L. Bullister, R. A. Feely, F. J. Millero, C. Mordy, T.-H. Peng, A global ocean carbon climatology: Results from Global Data Analysis Project (GLODAP). *Global Biogeochem. Cycles* **18**, GB4031 (2004).
70. R. N. Roy, L. N. Roy, K. M. Vogel, C. Porter-Moore, T. Pearson, C. E. Good, F. J. Millero, D. M. Campbell, The dissociation constants of carbonic acid in seawater at salinities 5 to 45 and temperatures 0 to 45°C. *Mar. Chem.* **44**, 249–267 (1993).
71. A. Mucci, The solubility of calcite and aragonite in seawater at various salinities, temperatures, and one atmosphere total pressure. *Am. J. Sci.* **283**, 780–799 (1983).
72. F. E. Grubbs, Procedures for detecting outlying observations in samples. *Dent. Tech.* **11**, 1–21 (1969).
73. D. de Beer, A. Glud, E. Epping, M. Kühl, A fast-responding CO_2 microelectrode for profiling sediments, microbial mats, and biofilms. *Limnol. Ocean.* **42**, 1590–1600 (1997).
74. P. S. Davies, Short-term growth measurements of corals using an accurate buoyant weighing technique. *Mar. Biol.* **101**, 389–395 (1989).
75. M. Guillermic, S. Misra, R. Eagle, A. Villa, F. Chang, A. Tripati, Seawater pH reconstruction using boron isotopes in multiple planktonic foraminifera species with different depth habitats and their potential to constrain pH and pCO_2 gradients. *Biogeosciences* **17**, 3487–3510 (2020).
76. M., Gutjahr, L., Bordier, E., Douville, J., Farmer, G. L., Foster, E., Hathorne, B. Hönisch, D. Lemarchand, P. Louvat, M. M. Culloch, J. Noireaux, N. Pallavicini, I. Rodushkin, P. Roux, J. Stewart, F. Thil, C.-F. You, Boron Isotope Intercomparison Project (BIIP): Development of a new carbonate standard for stable isotopic analyses, in *EGU General Assembly Conference Abstracts (Vol. 16)* (2014)
77. M. Holcomb, T. M. DeCarlo, V. Schoepf, D. Dissard, K. Tanaka, M. McCulloch, Cleaning and pre-treatment procedures for biogenic and synthetic calcium carbonate powders for determination of elemental and boron isotopic compositions. *Chem. Geol.* **398**, 11–21 (2015).
78. S. Misra, M. Greaves, R. Owen, J. Kerr, A. C. Elmore, H. Elderfield, Determination of B/Ca of natural carbonates by HR-ICP-MS. *Geochem. Geophys. Geosyst.* **15**, 1617–1628 (2014).
79. K. Klochko, A. J. Kaufman, W. Yao, R. H. Byrne, J. A. Tossell, Experimental measurement of boron isotope fractionation in seawater. *Earth Planet. Sci. Lett.* **248**, 261–270 (2006).
80. S. Barker, M. Greaves, H. Elderfield, A study of cleaning procedures used for foraminiferal Mg/Ca paleothermometry. *Geochem. Geophys. Geosyst.* **4**, 8407 (2003).
81. E. J. Catanzaro, C. E. Champion, A. L. Garner, G. Marinenko, K. M. Sappenfield, W. R. Shields, Boric Acid; Isotopic and Assay Standard Reference Materials (U.S. Natl. Bur. Stand. Spec., Publ., 1970), pp. 260–17, 70p.
82. O. Nir, A. Vengosh, J. S. Harkness, G. S. Dwyer, O. Lahav, Direct measurement of the boron isotope fractionation factor: Reducing the uncertainty in reconstructing ocean paleo-pH, Earth Planet. *Sci. Lett.* **414**, 1–5 (2015).
83. J. Gaillardet, D. Lemarchand, C. Göpel, G. Manhès, Evaporation and sublimation of boric acid: Application for boron purification from organic rich solutions. *Geostand. Newsl.* **25**, 67–75 (2001).
84. B.-S. Wang, C.-F. You, K.-F. Huang, S.-F. Wu, S. K. Aggarwal, C.-H. Chung, P.-Y. Lin, Direct separation of boron from Na- and Ca-rich matrices by sublimation for stable isotope measurement by MC-ICP-MS. *Talanta* **82**, 1378–1384 (2010).
85. S. Misra, R. Owen, J. Kerr, M. Greaves, H. Elderfield, Determination of δ^{11}B by HR-ICP-MS from mass limited samples: Application to natural carbonates and water samples. *Geochim. Cosmochim. Acta* **140**, 531–552 (2014b).
86. J. W. B. Rae, Boron isotopes in Foraminifera: Systematics, biomineralisation, and CO_2 reconstruction, in *Boron Isotopes. Advances in Isotope Geochemistry*, H. Marschall, G. Foster, Eds. (Springer, 2018).
87. M. Raitzsch, J. Bijma, A. Benthien, K.-U. Richter, G. Steinhoefel, M. Kučera, Boron isotope-based seasonal paleo-pH reconstruction for the Southeast Atlantic – A multispecies approach using habitat preference of planktonic foraminifera. *Earth Planet. Sci. Lett.* **487**, 138–150 (2018).
88. N. S. Lloyd, A. Y. Sadekov, S. Misra, Application of 10^{13} ohm Faraday cup current amplifiers for boron isotopic analyses by solution mode and laser ablation multicollector inductively coupled plasma mass spectrometry. *Rapid Commun. Mass Spectrom.* **32**, 9–18 (2018).

Acknowledgments
Funding: R.A.E. and J.B.R. acknowledge support from National Science Foundation grants OCE-1437166 and OCE-1437371. The work was also supported by the "Laboratoire d'Excellence" LabexMER (ANR-10-LABX-19), cofunded by a grant from the French government under the program "Investissements d'Avenir," and an IAGC student grant 2017. R.A.E. acknowledges financial and logistical support from the Pritzker Endowment to UCLA IoES, and J.B.R. acknowledges support from the ZMT and the Hanse-Wissenschaftskolleg Fellowship Program and the NSF OCE award #1437371. We thank C. Bouniol for assistance with sample preparation and Y. Germain and C. Liorzou for technical assistance. We thank the staff of the ZMT experimental aquaria facility for their support, without which this study would not have been possible. We thank J. Sutton and J. Drake for providing comments on a draft of this manuscript. **Author contributions:** R.A.E. and J.B.R. conceived the project and directed the research. L.P.C. and J.B.R. performed culturing experiments, specimen characterization, and pH microsensor experiments with input from D.d.B., C.E.R., H.W., and R.A.E. M.G., I.D.C., and S.M. performed isotope and trace element analyses at the University of Cambridge and the University of Brest, and J.B. oversaw isotope analyses at Bremerhaven. M.G., S.M., R.A.E., J.B., and J.B.R. analyzed and interpreted the geochemical data. M.G. wrote the manuscript with input from R.A.E. and J.B.R. All authors read and edited the manuscript. **Competing interests:** The authors declare that they have no competing interests. **Data and materials availability:** All data needed to evaluate the conclusions in the paper are present in the paper and/or the Supplementary Materials. Additional data related to this paper may be requested from the authors.

Submitted 22 January 2020
Accepted 11 November 2020
Published 8 January 2021
10.1126/sciadv.aba9958

Citation: M. Guillermic, L. P. Cameron, I. De Corte, S. Misra, J. Bijma, D. de Beer, C. E. Reymond, H. Westphal, J. B. Ries, R. A. Eagle, Thermal stress reduces pocilloporid coral resilience to ocean acidification by impairing control over calcifying fluid chemistry. *Sci. Adv.* **7**, eaba9958 (2021).